R-04-03

Äspö Pillar Stability Experiment

Final coupled 3d thermo – mechanical modeling

Preliminary particle – mechanical modeling

Toivo Wanne, Erik Johansson, David Potyondy
Saanio & Riekkola Oy

February 2004

Svensk Kärnbränslehantering AB
Swedish Nuclear Fuel
and Waste Management Co
Box 5864
SE-102 40 Stockholm Sweden
Tel 08-459 84 00
+46 8 459 84 00
Fax 08-661 57 19
+46 8 661 57 19

ISSN 1402-3091
SKB Rapport R-04-03

Äspö Pillar Stability Experiment

Final coupled 3d thermo – mechanical modeling

Preliminary particle – mechanical modeling

Toivo Wanne, Erik Johansson, David Potyondy
Saanio & Riekkola Oy

February 2004

Keywords: Äspö HRL, Thermo-mechanical modeling, Particle-mechanical modeling, Coupling, FLAC/FLAC3D, PFC2D, Nuclear waste disposal, Pillar stability, Damage, Thermal stresses.

Abstract

SKB is planning to perform a large-scale pillar stability experiment called APSE (Äspö Pillar Stability Experiment) at Äspö HRL. The study is focused on understanding and control of progressive rock failure in hard crystalline rock and damage caused by high stresses.

The elastic thermo-mechanical modeling was carried out in three dimensions because of the complex test geometry and in-situ stress tensor by using a finite-difference modeling software FLAC3D. Cracking and damage formation were modeled in the area of interest (pillar between two large scale holes) in two dimensions by using the Particle Flow Code (PFC), which is based on particle mechanics. FLAC and PFC were coupled to minimize the computer resources and the computing time.

According to the modeling the initial temperature rises from 15°C to about 65°C in the pillar area during the heating period of 120 days. The rising temperature due to thermal expansion induces stresses in the pillar area and after 120 days heating the stresses have increased about 33% from the excavation induced maximum stress of 150 MPa to 200 MPa in the end of the heating period.

The results from FLAC3D model showed that only regions where the crack initiation stress has exceeded were identified and they extended to about two meters down the hole wall. These could be considered the areas where damage may occur during the in-situ test. When the other hole is pressurized with a 0.8 MPa confining pressure it yields that 5 MPa more stress is needed to damage the rock than without confining pressure. This makes the damaged area in some degree smaller.

High compressive stresses in addition to some tensile stresses might induce some AE (acoustic emission) activity in the upper part of the hole from the very beginning of the test and are thus potential areas where AE activities may be detected. Monitoring like acoustic emissions will be measured during the test execution.

The 2D coupled PFC-FLAC modeling indicated that microcracks/damages are localized and formed asymmetrically (distributed fractures around the holes). However, these results confirm even in spite of the facts that very few laboratory tests in respect to the area of interest were conducted to characterize the rock properties and that pillar is assumed to be geologically homogeneous, that at least some damages and microcracking shall be formed in rock in the pillar area of interest, which was one of the the main objectives in the pillar stability experiment.

Sammanfattning

SKB planerar att genomföra ett storskaligt pelarstabilitetsexperiment benämnt APSE (Äspö Pillar Stability Experiment) vid Äspölaboratoriet. Studien fokuserar på förståelse och kontroll av progressivt brott i hårt kristallint berg samt de skador som uppstår genom höga bergspänningar.

Den kopplade elastiska termomekaniska modelleringen utfördes i tre dimensioner på grund av den komplexa experimentgeometrin genom att använda det finita differensprogrammet FLAC3D. Sprickbildningen och skadornas omfattning i pelaren modellerades även i två dimensioner genom att använda Particle Flow Code (PFC) som baserar sig på partikelmekanik. FLAC och PFC programmen kopplades till varandra vid körningarna för att spara på datorresurser och beräkningstid.

Enligt modelleringen kommer den initiella temperaturen i pelarvolymen att öka från 15 grader till cirka 65 grader under de 120 dygn som värmarna planeras att vara driftsatta. Efter de 120 dygnen kommer den termiska expansion av berget att ge upphov till tillskottsspänningar som ökar den totala lasten på pelarväggen med cirka 33 %. Efter det att de båda hålen borrats kommer den maximala tillförda spänningen att vara cirka 150 MPa för att i värmningsfasens slutskede nå cirka 200 MPa.

Resultaten från FLAC3D modelleringarna visar att och var lasten kommer att gå över crack initiation strength. Detta kommer att ske från sulan och cirka 2 meter ned utefter pelarväggen och det är detta område som skadorna förväntas att ske under fältförsöket. Eftersom ett av hålen är trycksatt med 0,8 MPa övertryck så kommer det att krävas cirka 5 MPa högre bergspänningar för att inducera brott i det hålet jämfört med det tomma. Det skadade området kommer därför att var något mindre i det trycksatta hålet.

Höga tryckspänningar tillsammans med dragspänningar kan ge upphov till AE (acoustic emission) aktivitet i den övre delen av hålet i ett tidigt skede av experimentet. AE kommer att vara ett av de instrumentsystem som kommer att övervaka experimentet.

Den kopplade 2D PFC-FLAC modelleringen påvisar att mikrosprickbildning kommer att initieras och utvecklas asymmetriskt runt hålen. Trots att endast ett fåtal laboratorietest utförts för att karakterisera experimentområdet samt att pelaren antages vara homogen bekräftar modelleringen att mikrosprickbildning i någon form kommer att ske i pelaren. Detta är en viktig slutsats eftersom det är en av de huvudsakliga målsättningarna med experimentet.

Contents

1 Introduction

1.1 General

SKB is preparing to perform a large-scale pillar stability experiment (APSE) at Äspö HRL /Andersson, 2003/. Damages caused by temperature-induced stresses will be studied in the APSE. The objectives are set by SKB:

1. Demonstrate the capability to predict spalling in a fractured rock mass.
2. Demonstrate the effect of backfill (confining pressure) on the rock mass response.
3. Comparison of 2D and 3D mechanical and thermal predicting capabilities.

The field experiment will be carried out in summer 2004. The pre-test modeling was done previously by /Wanne and Johansson, 2003; Fredriksson et al. 2003; Rinne et al. 2003/ and this one presented here supports also technical feasibility study of the planned experiment. The elastic modeling was carried out in three dimensions because of the complex test geometry and in-situ stress tensor by using a finite-difference modeling software FLAC3D. Cracking and damage formation were modeled in two dimensions with a novel approach of coupled particle-mechanic – continuum code PFC-FLAC.

This report describes the final thermal and mechanical modeling of the pillar experiment by using FLAC3D /Itasca, 2002/ and coupled PFC-FLAC /Itasca, 2003/.

Input data for modeling was submitted by SKB.

1.2 APSE large-scale in-situ experiment

The geometry of the in-situ failure test is presented in Figure 1-1. The tunnel width is 5 meter and height is 7.5 meter. The tunnel floor is curved with a radius of 2 meters. In the tunnel floor, two 8 meters deep boreholes (diameter 1.8 m) will be bored. The hole dimensions correspond to the spent nuclear fuel waste deposition hole. There is 1 meter wide rock section between the holes. The other disposal hole is pressurized to 0.8 MPa by a bladder to simulate the backfilling effect. The confinement is decreased at the end of the in-situ test to study the level of the backfilling pressure, which restrains the damage/micro-cracking forming in the rock.

The rock mass is heated by four heaters placed in boreholes around the test area (see Figure 1-1). The heating expands the rock, which increases the stresses at the area of interest. These stresses are planned to be high enough to cause damage to occur in the pillar area.

The fracturing and damage forming will be monitored visually, with mechanical sensors, and with acoustic emission sensors. The in-situ test out-come is finally compared with the modeled behavior of the test. Also, some post-experiment characterization is planned to be done.

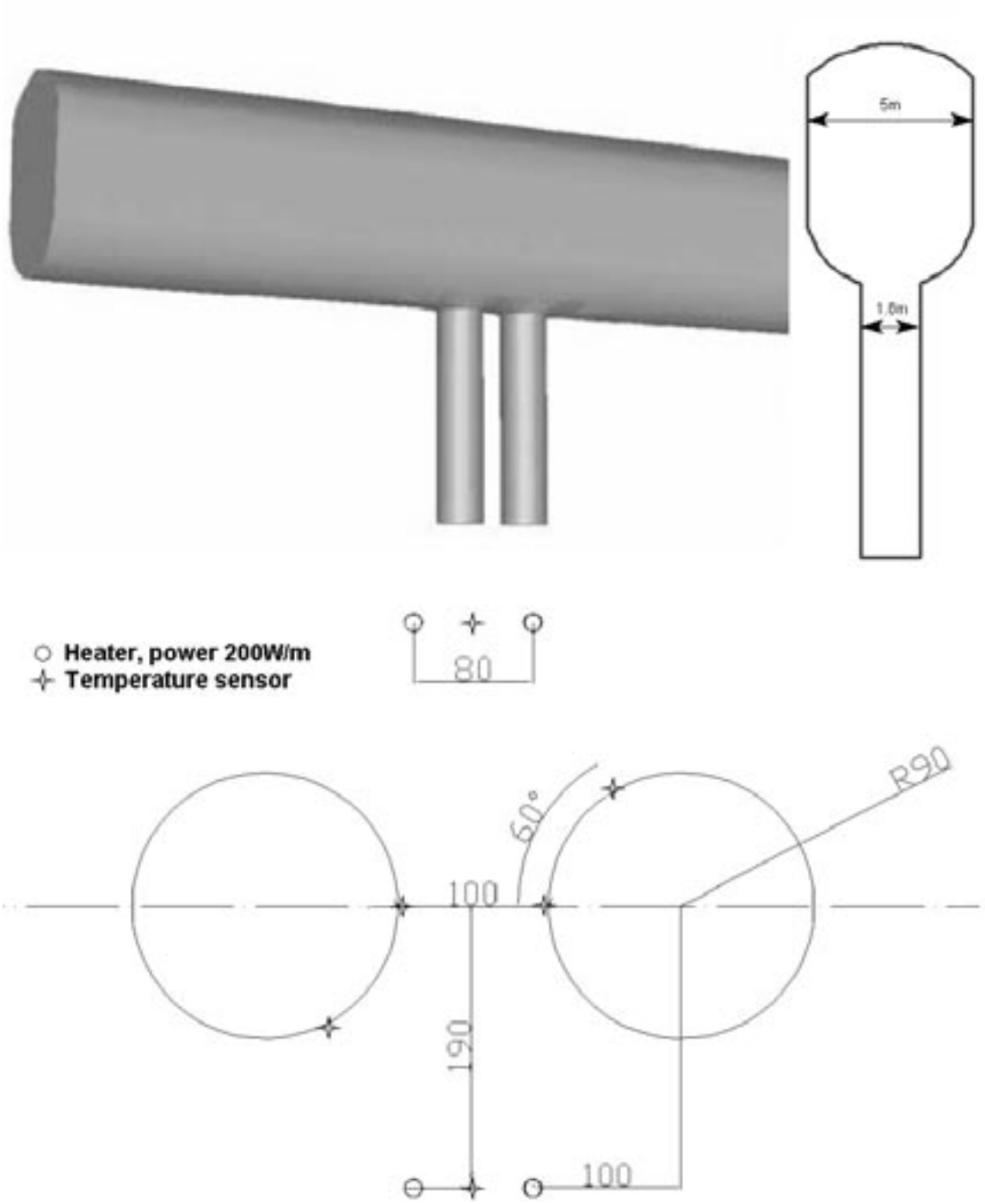

Figure 1-1. *Original geometry of the APSE experiment. The tunnel floor is curved. Two full-scale deposition holes are drilled, diameter 1.8 m, depth 8.0 m with a distance of 1.0 meter. Area between the holes is called the pillar.*

2 FLAC3D modeling

2.1 Software

The thermal and mechanical modeling computations were performed using Itasca's FLAC3D software /Itasca, 2002/. FLAC3D is a three-dimensional finite-difference program using explicit solution scheme for engineering mechanics computation. Software simulates the behavior of three-dimensional structures built of soil, rock or other materials that undergo plastic flow when their yield-limits are reached. The geometry is modeled by using polyhedral elements within a three-dimensional grid that is adjusted to fit the shape of the object to be modeled.

Material model used in this study was elastic. The used isotropic thermal model simulates the transient flux of heat in materials and the subsequent development of thermally induced stresses. The thermal-mechanical coupling is one-way; temperature change may induce a mechanical stress change, however mechanical changes in the body do not result temperature changes. Software contains also a powerful built-in programming language, FISH, which was used to individually tailored analyses.

Preliminary modeling for APSE has been earlier performed also with FLAC3D and results are presented in /Wanne and Johansson, 2003/.

2.2 Model geometry

The model geometry is created as a grid in a global x, y, z-coordinate system. The model geometry is assembled by using a library of primitive mesh shapes and p utting them together. The APSE model is constructed by using three different shapes (radial cylinder, radial tunnel, and brick). The model is 50 m wide, 37 m high, and 30 m in length. The tunnel is oval-shaped with width of 5 m and the height of 7.5 m. The 1.8 m diameter disposal holes are situated at the tunnel floor in the middle of the model. The model grid zone size is smallest (5 × 15 × 25 cm) at the pillar area, which is the main area of interest. Elsewhere the zone size is larger to optimize the needed computational resources. The model has about 94,000 gridpoints and 86,000 zones. The model is shown in Figure 2-1.

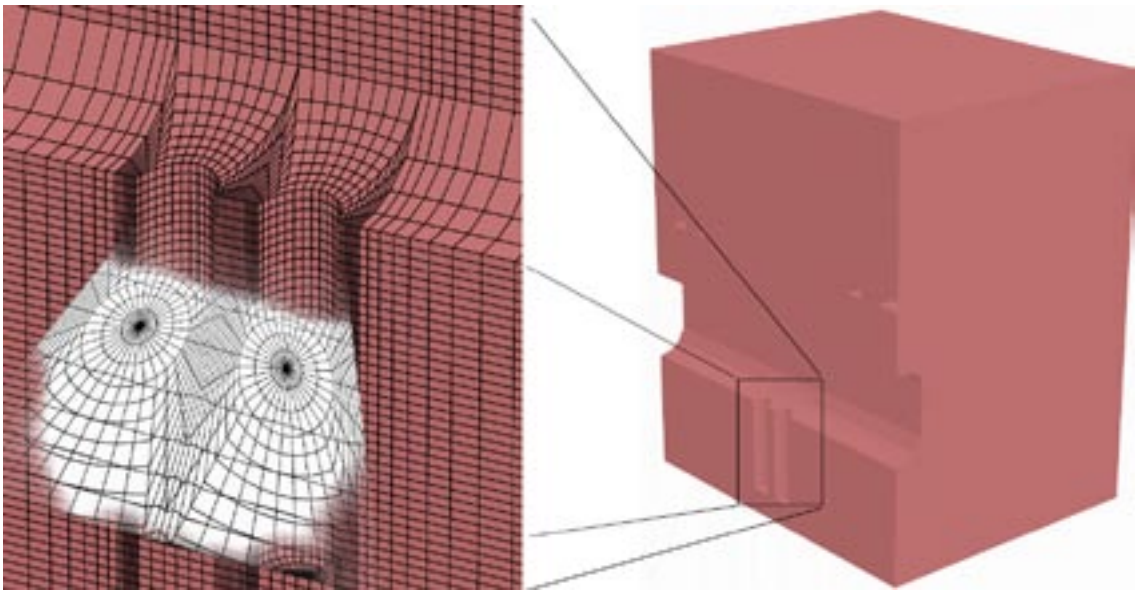

Figure 2-1. *Half FLAC3D model and magnification around the pillar area.*

2.3 Mechanical material properties

After the preliminary modeling phase additional laboratory tests on core samples from the test site and tunnel characterization have been performed /Barton, 2003/. SKB then submitted the material properties used in the modeling to each modeling group. Material properties describe Äspö diorite, which is considered the main rock type in the experimental area.

Material model used in FLAC3D simulations was elastic. Table 2-1 lists the obtained material properties determined at laboratory (intact rock) and based on the tunnel characterization (rock mass). The deformation properties of rock mass values were used in the modeling. The model describes unfractured rock but it should be noted that the actual test site was found to be fractured. In addition, a shear zone (altered rock with uniaxial strength of only about 130 MPa) that intersected the pillar was observed.

The uniaxial strength of the rock was fixed to be 210 MPa, the crack damage strength 204 MPa, the crack initiation strength 121 MPa, and the tensile strength 14.3 MPa /Staub et al. 2004/. The available test data was used in the fitting of values to the failure criterion (see Section 3.4).

Table 2-1. Mechanical material properties of Äspö diorite, intact rock and rock mass /Staub et al. 2004/.

Young's modulus, E [GPa]		**Poisson's ratio, v**	
75.0	**55.0**	**0.25**	**0.26**
intact – rock mass		**intact – rock mass**	
Uniaxial peak strength	210 MPa		
Crack damage stress	204 MPa		
Crack initiation stress	121 MPa		
Tensile strength	14.3 MPa		

2.4 Thermal loading

The in-situ test area is heated with four heaters. The layout is shown in Figure 1-1. The heaters are situated in vertical boreholes and are 6.5 meters long. The unit heating power is 200 W/m. The rock mass is planned to be heated 120 days during which time the temperature-induced stresses should have reached high-enough values to initiate fracturing.

Detailed formulation of the thermal calculation in FLAC3D can be found in the software manuals /Itasca, 2002/. The used thermal properties are listed in Table 2-2.

Heater effect is set to be 200 W/m. Hence each of the four heaters has an total effect of 1,300 W (=6.5 m × 200 W/m) per heater.

In addition, several thermocouples will be installed in boreholes in the test area to monitor the temperature development during the heating. In FLAC3D model temperature histories were surveyed at the same locations so they can be compared later with the measured ones. There are six temperature monitoring arrays installed, each with four locations at different depths.

By default, in thermal modeling, all the boundaries and free surfaces in the model are adiabatic i.e. fully insulated. Convection of the heat to the tunnel air was not included in the modeling. This is not considered significant since the holes will be covered by lid during the in-situ test.

2.5 Stress state

Two key design factors to increase the stresses in the pillar area were the geometry of floor and the orientation of tunnel (perpendicular to the major principal stress). The in-situ stress state at site is presented in Table 2-3. The values are based on the in-situ stress measurements and back-analyses calculated from the tunnel convergence measurements /Staub et al. 2004/.

The model is subjected to the in-situ stress state, which prevails in the test site. The stresses were applied to the model as boundary conditions and as initial stresses in every zone. Before the actual modeling the model was set to equilibrium under the given boundary and initial conditions.

Table 2-2. Thermal properties of the FLAC3D model /Staub et al. 2004/.

Density, ρ [kg/m^3]	Conductivity, K [W/m, K]	Heat capacity, [MJ/m^3, K]	Linear exp. coeff., αt [1/°C]
2,750	**2.60**	**2.1**	**7.0×10^{-6}**
Specific heat, Cv [J/kg, K]	**775**	Initial temperature [°C]	**15.0**

Table 2-3. In-situ stress state used in the modeling.

Stress component	Magnitude [MPa]	Dip direction [°]	Dip [°]
σ1	27	310	07
σ2	10	090	83
σ3	10	208	00

APSE tunnel orientation is 046°.

3 Results of FLAC3D thermal – mechanical modeling

3.1 Pre-heating stage

The geometry and orientation of the test tunnel cause high stress field in the pillar area as it was planned. Figure 3-1 shows the stress field around the test tunnel opening. The holes are not yet excavated. The maximum stresses are over 70 MPa at the tunnel floor. The induced stress field is slightly inclined and off-centered at the floor. This is due to input stress tensor (see Table 2-3).

Boring the first full-scale disposal hole increases the stresses at the top of the pillar from 75 MPa to 160 MPa. Figure 3-2 shows the maximum principal stresses at the pillar area. The highest stresses are about 165 MPa and located at the top of the pillar. Stress values decrease at the deeper depths being about 140 MPa at the depth of 0.5 m. Boring the second hole increases slightly the magnitude of stresses and make them uniform at the pillar area. Cross-section from the level 0.5 meters below the tunnel floor shows that the stresses concentrate on the pillar-side hole wall (Figure 3-3). Maximum stress at that level is about 140 MPa.

The maximum stress at the pillar is about five-times the initial in-situ principal stress due the tunnel geometry and hole excavations.

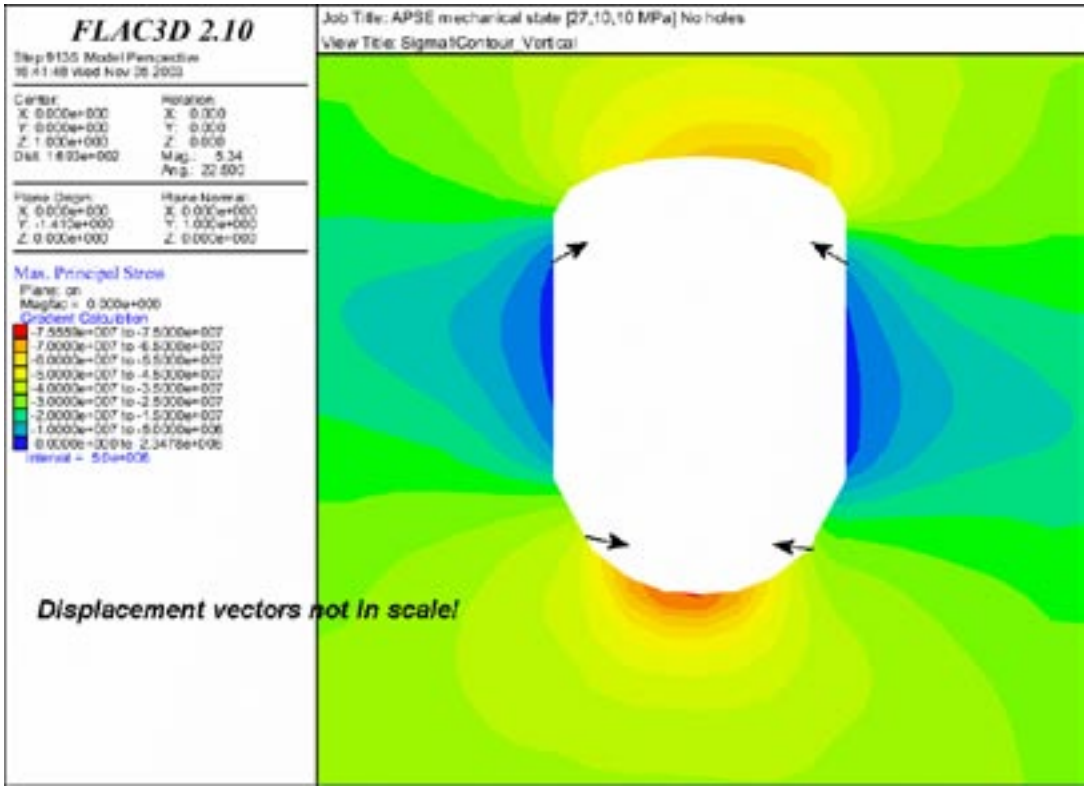

Figure 3-1. *Tunnel geometry and orientation concentrate the highest stresses at the floor area. Maximum stress is about 75 MPa at the floor surface. Displacement vectors are for general information only and not in any scale.*

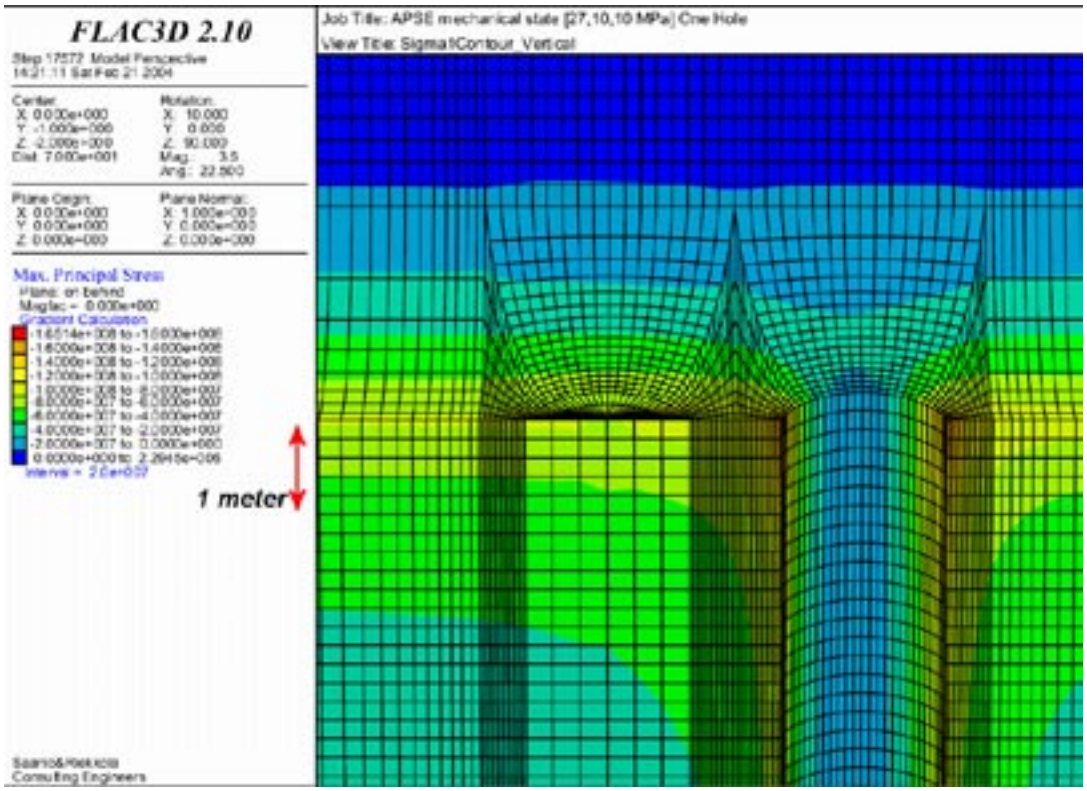

Figure 3-2. *Vertical section parallel to the axis of APSE tunnel showing the experimental area after boring of the first hole and lower part of the tunnel wall and the top 5 meters of the bored hole. Maximum principal stress at the top of the pillar is about 160 MPa. No heating.*

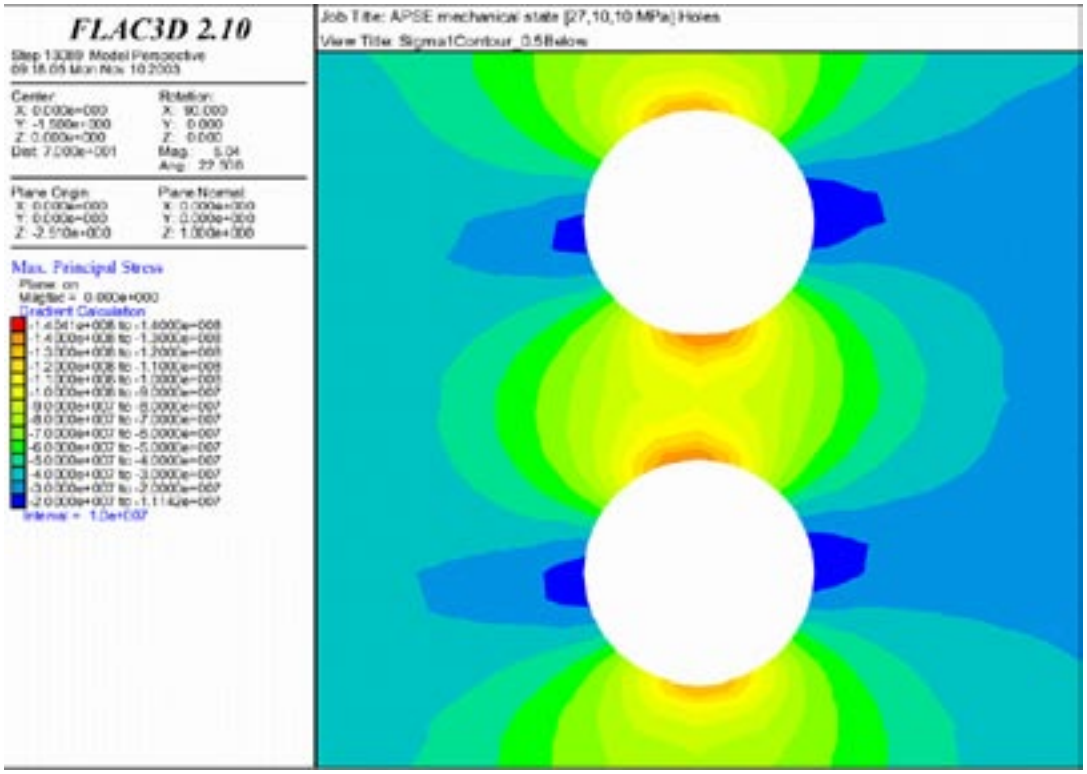

Figure 3-3. *Horizontal cross section at the level 0.5 meters below the tunnel floor with both holes shows that the stresses concentrate to the pillar wall. Maximum principal stress at the wall is about 140 MPa. No heating.*

3.2 Temperature field

The rock mass is heated by four heaters placed around the experimental volume. Heating expands the rock mass, thus increases the stresses at the pillar area. The heating time in the modeling was 120 days. The temperature was monitored in the model during the heating period in various locations. The layout of the temperature sensor arrays is shown in Figure 3-4. The temperature reading was taken at various depths as stated in corresponding graphs (0 m corresponds temperature reading at tunnel floor, 6.5 m corresponds temperature reading from a sensor at 6.5 meters depth below tunnel mid floor). Figures 3-5 through 3-8 show the temperatures graphs from the heating period of 120 days.

After 120 days of heating temperature rises up to 70 degrees Celsius at the pillar area, as the initial temperature was 15 degrees. At the lower part of the pillar temperature is in around 40 degrees. The fact that the heaters are over a meter shorter than the disposal hole can be seen in Figure 3-9, which shows temperature field at the mid-pillar cross section. The temperature at the bottom of the holes stays near the set initial temperature.

Tunnel floor is planned to be covered during the in-situ test and therefore air convection was not taken into account in the modeling.

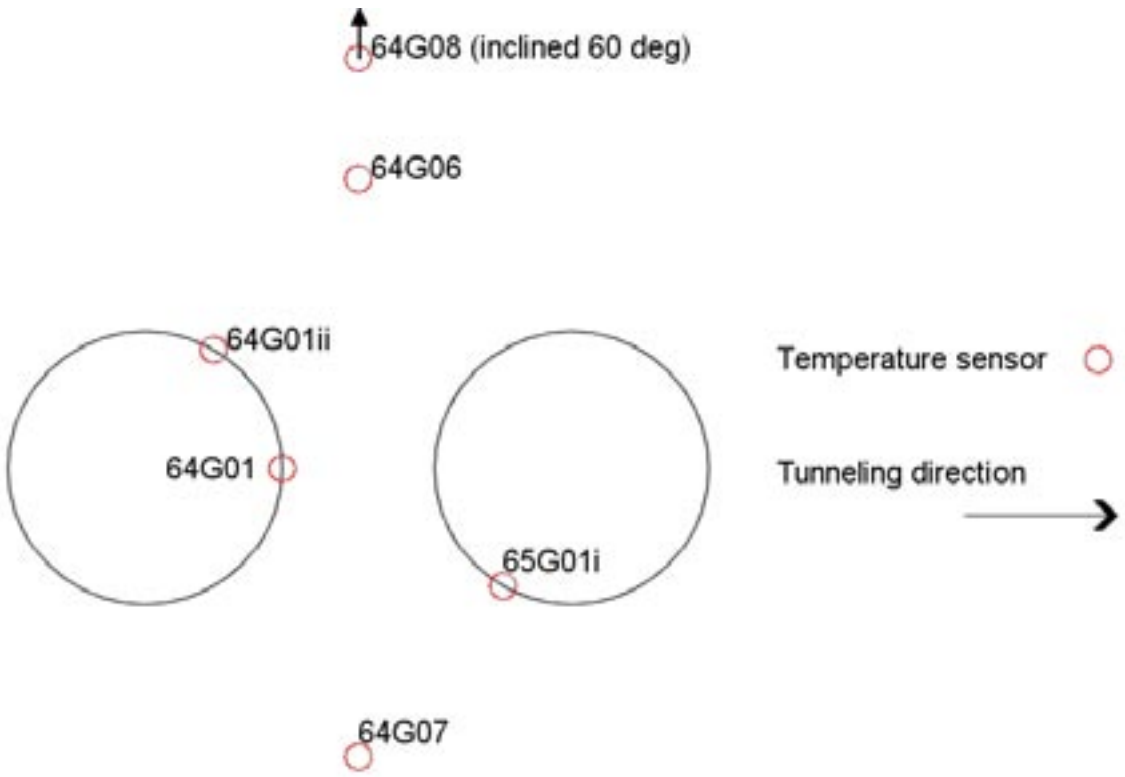

Figure 3-4. *Layout of the temperature sensor arrays. Three sets of arrays were placed in core-drilled holes, and three sets of arrays at disposal hole walls.*

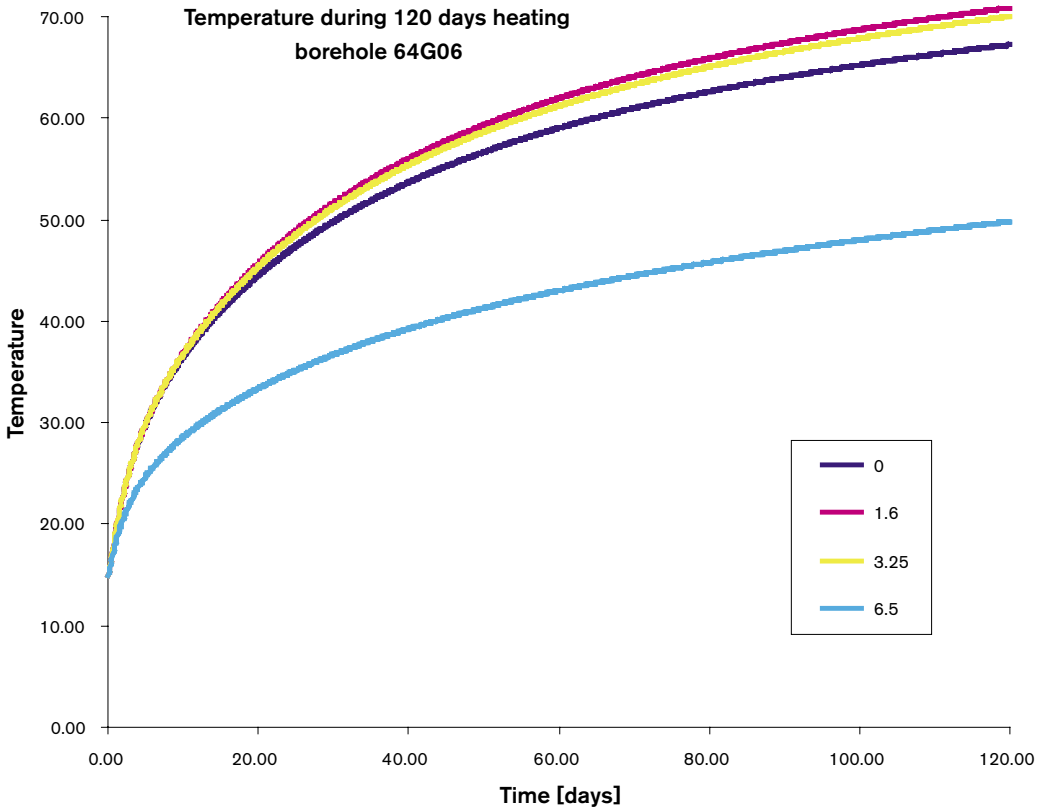

Figure 3-5. *Temperature in °C at different depths during the heating period between the heater set 1. Same as for array in borehole KQ0064G07.*

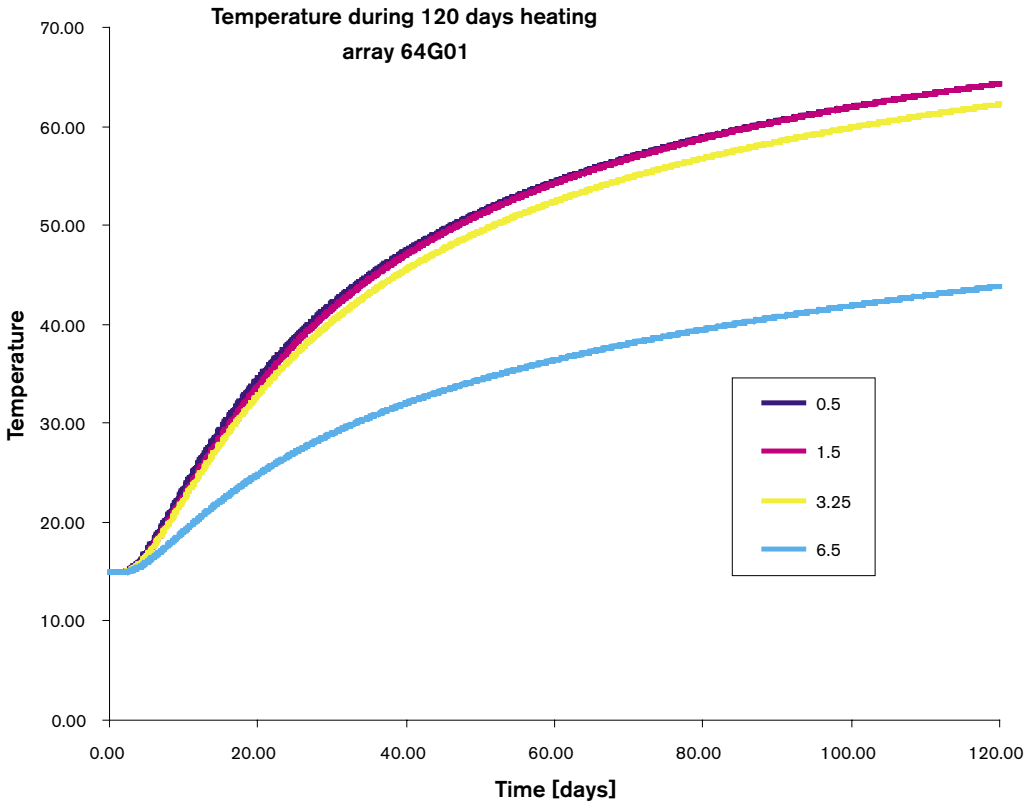

Figure 3-6. *Temperature in °C at different depths during the heating at the first disposal hole wall, array 64G01.*

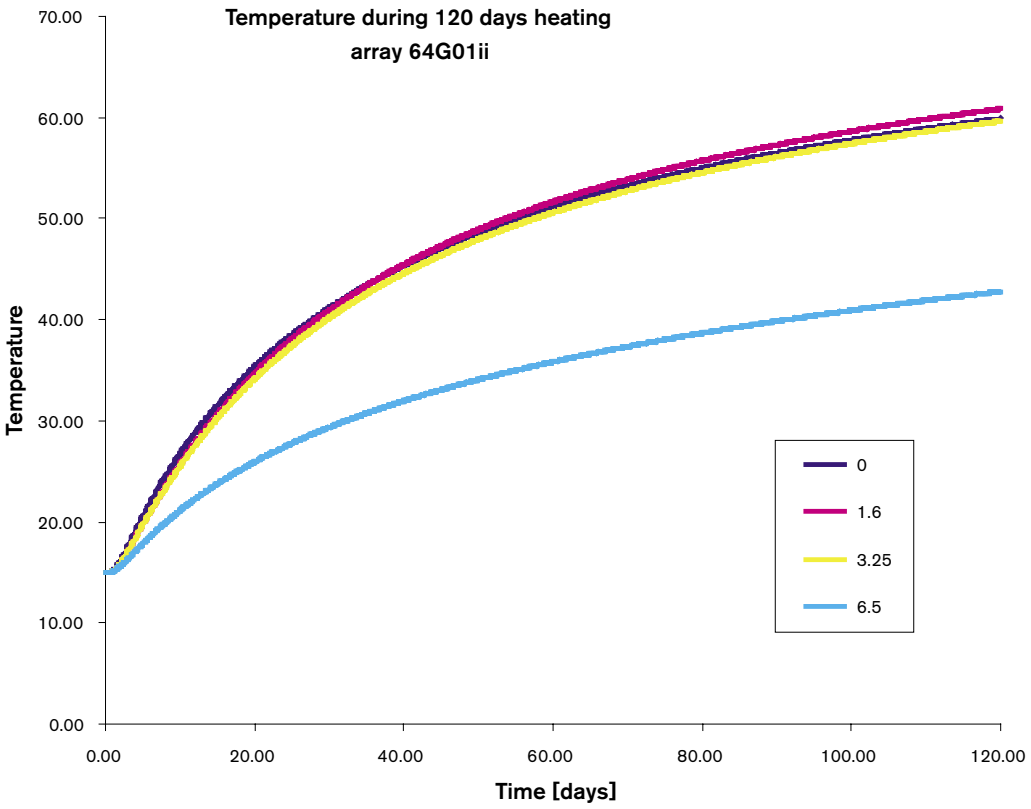

Figure 3-7. *Temperature in °C at different depths during the heating at the first disposal hole wall, array 64G01ii.*

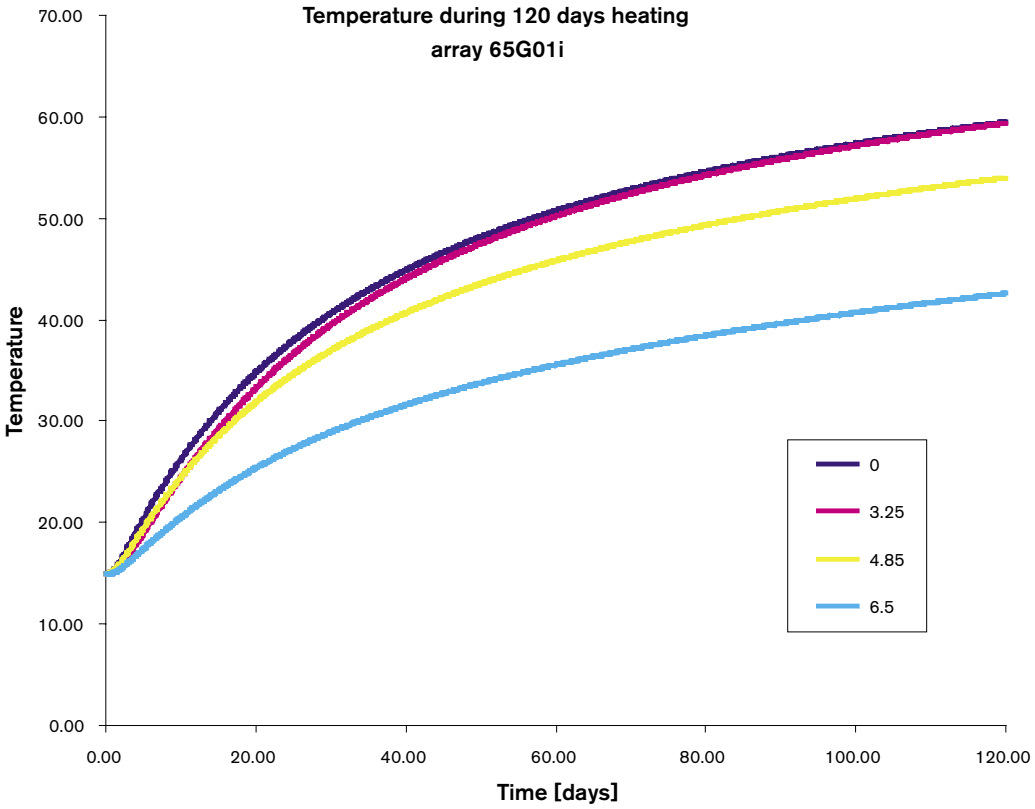

Figure 3-8. *Temperature in °C at different depths during the heating at the second disposal hole wall, array 65G01i.*

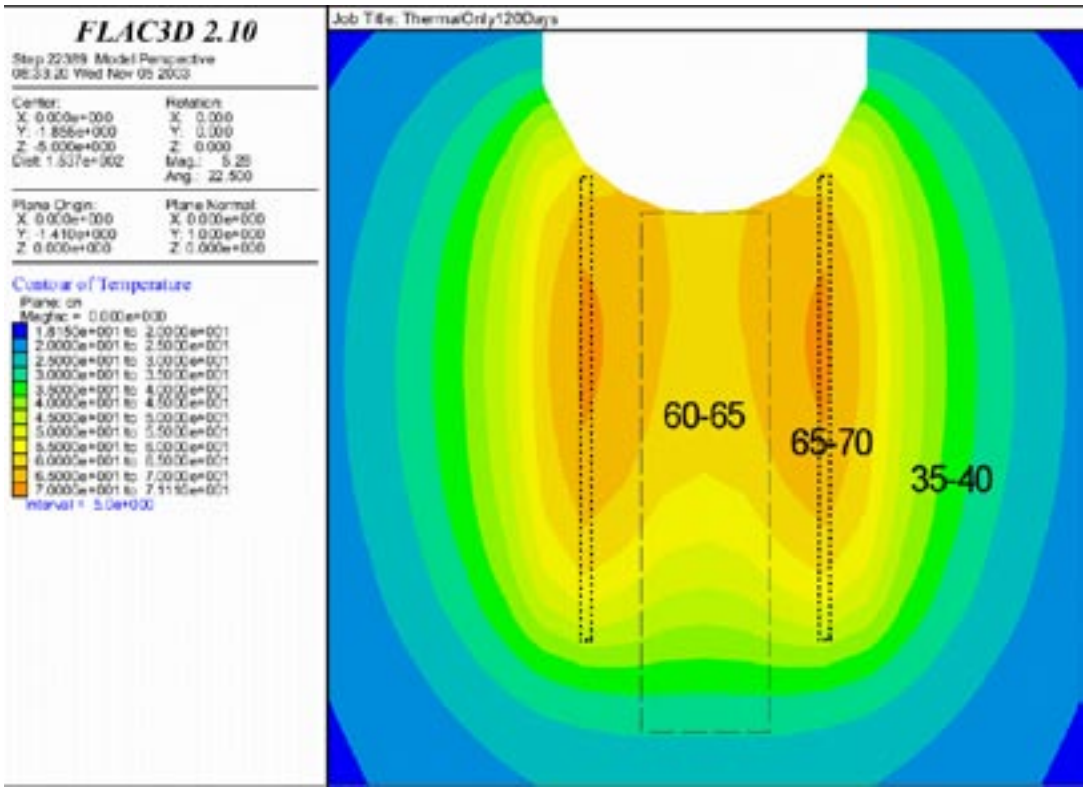

Figure 3-9. *Temperature field at the vertical mid-pillar cross section after 120 days heating. Borehole and heater locations are marked with dashed and dotted lines.*

3.3 Stress field

Heating expands the rock mass and increases stresses. The heating (ΔT) effect on stress increase ($\Delta\sigma$) can be estimated with Equations 3-1 and 3-2. Using given material properties (see Chapter 2 Tables 2-1 and 2-2) and assuming the temperature increase of 50 degrees, the temperature-induced stress increase would be around 50 MPa.

$$\Delta\sigma = 3 \times K \times \alpha_t \times \Delta T \tag{3-1}$$

$$K = \frac{E}{3(1-2\times\upsilon)} \tag{3-2}$$

The highest increase of stress occurs at the upper part of pillar. Stresses down at the hole sidewalls are in same magnitude as at the pre-heating phase. Figure 3-10 shows the stress field after 120 days of heating at the tunnel half section. Figures 3-11 and 3-12 show the maximum principal stress field at the level of 0.5 m and 1.5 m below the tunnel floor, respectively. The highest stress values decrease at the deeper depths; at the level of 0.5 m the highest stress is 188 MPa and 1 meter below that 158 MPa.

The heating increases the stresses at the upper pillar area significantly. After 120 days of heating the stress increase at the level of 0.5 m below the floor is near 50 MPa. Maximum stresses at the top of the pillar are about 200 MPa (close the uniaxial crack damage stress) compared to 150 MPa without heating. Both, however, exceeds the uniaxial crack initiation stress level.

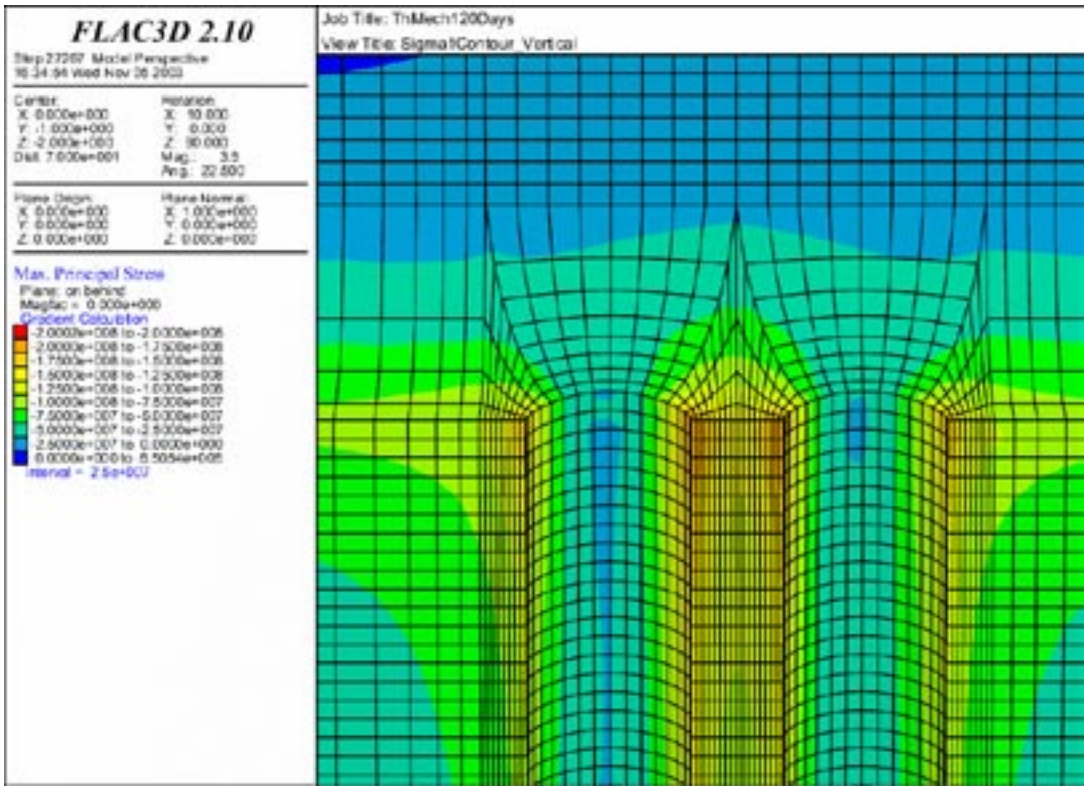

Figure 3-10. *Half section of the experimental area shows lower part of the tunnel wall and the top 5 meters of the bored holes. Maximum principal stress at the top of the pillar is about 200 MPa after the heating.*

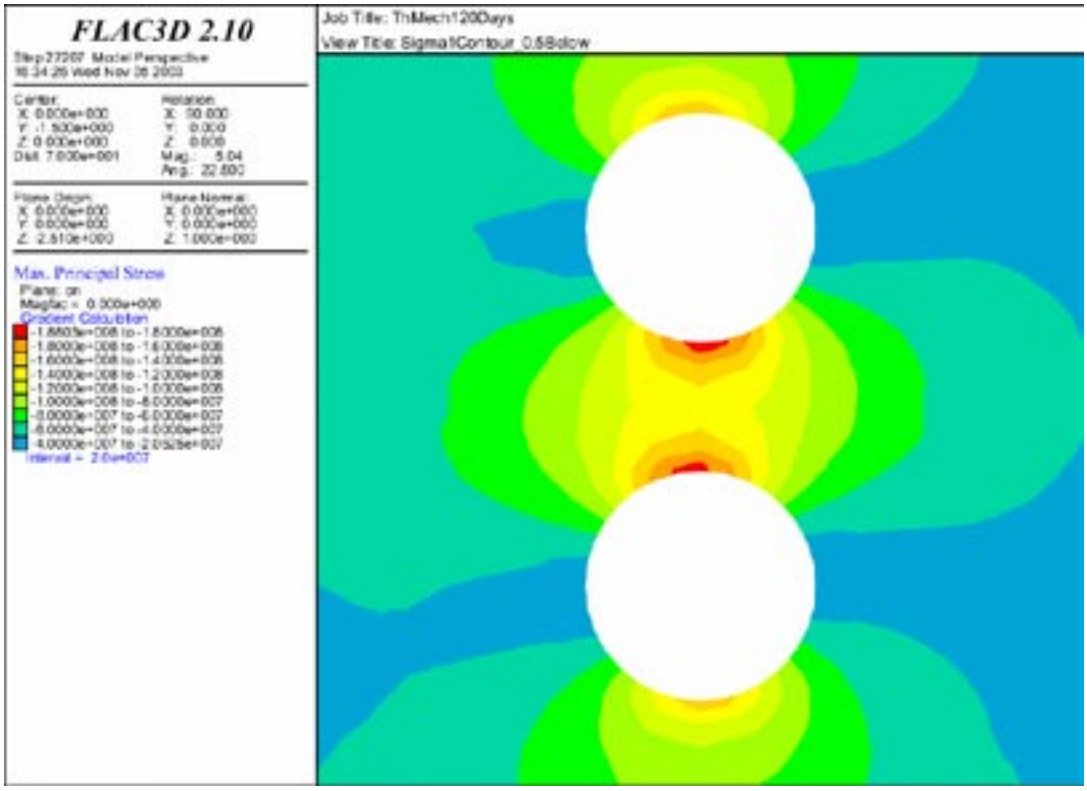

Figure 3-11. *Horizontal cross section at the level 0.5 meters below the tunnel floor shows that the stresses concentrate to the pillar wall. Maximum principal stress at the wall is about 188 MPa after 120 days heating.*

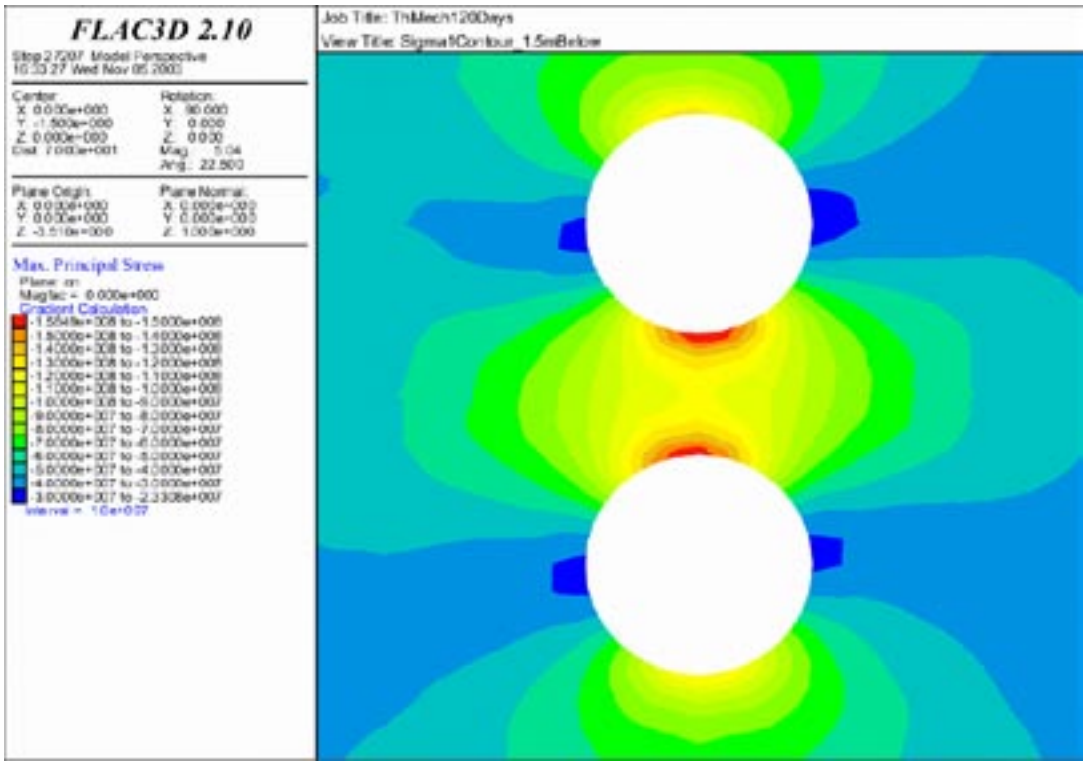

Figure 3-12. *Horizontal cross section at the level 1.5 meters below the tunnel floor. The maximum stress, about 158 MPa, is somewhat lower than at 1 meter above.*

3.4 Displacements

The elastic FLAC3D model deforms as the stress field changes. The deformation is fully linear and reversible, and related to the deformation modulus of the material. The displacements at the experimental area are in order of 1–2 mm (mainly upwards). The top of the pillar heaves about 1.5 mm. The hole deforms to an elliptical shape as most of the hole wall deformation occurs at the sidewalls. Figure 3-13 shows displacement vectors and contours in tunnel half section.

There were placed 18 displacement monitoring points for displacement at the hole wall (at the level 0.5 m below floor) that recorded the displacements (length of 3D-displacement vector) during entire modeling process. Figure 3-14 presents displacement history graphs. Figure 3-15 presents the displacement magnitudes as a function of the hole angle. The major part of the displacement is upward movement at the upper part of the pillar. Maximum horizontal component of the displacements is about 1.5 mm at the level 0.5 m below floor. The displacements at the level 1.5 m are only little smaller than at 0.5 m level.

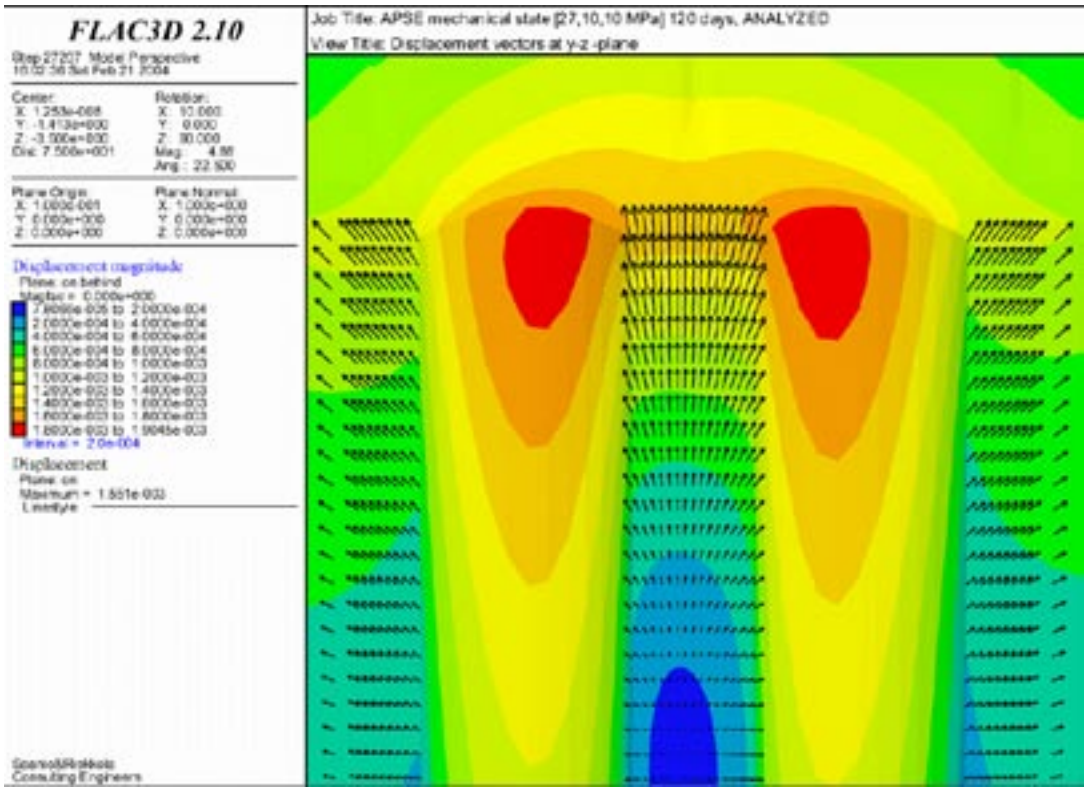

Figure 3-13. *Model after 120 days heating. Displacement vectors at mid-tunnel plane (max. 1.5 mm) and displacement magnitude contour at tunnel half section (max 1.9 mm). The major displacement vector component is upwards.*

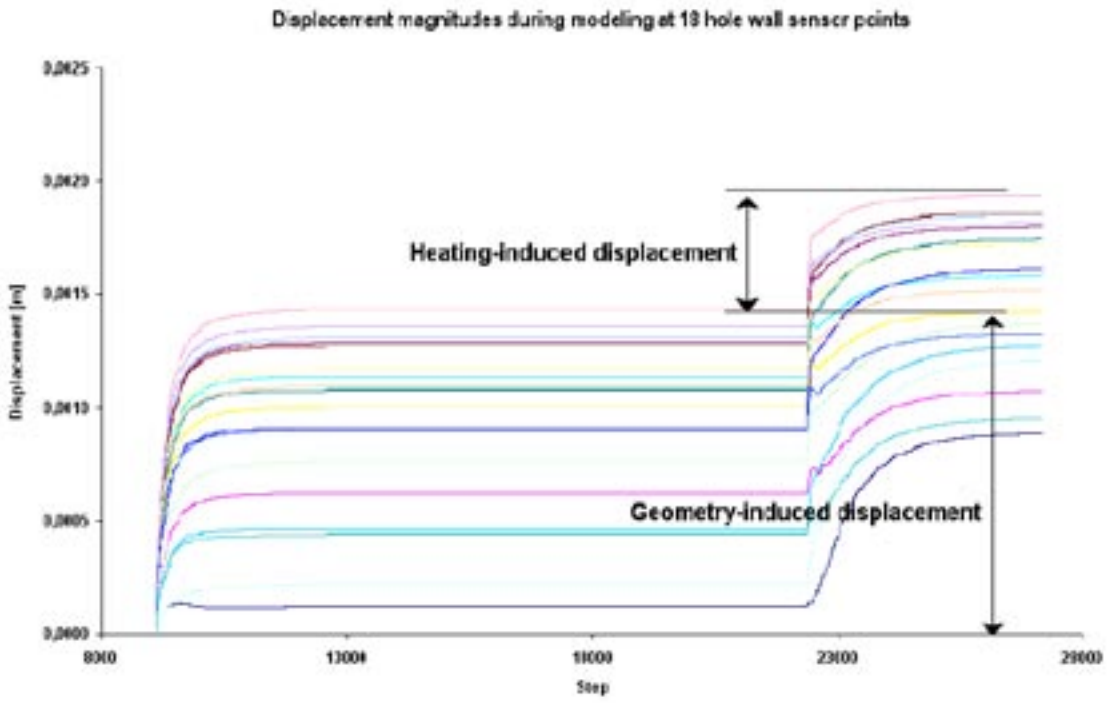

Figure 3-14. *Displacements of 18 monitoring points during the modeling process located at the hole wall 0.5 m below the tunnel floor.*

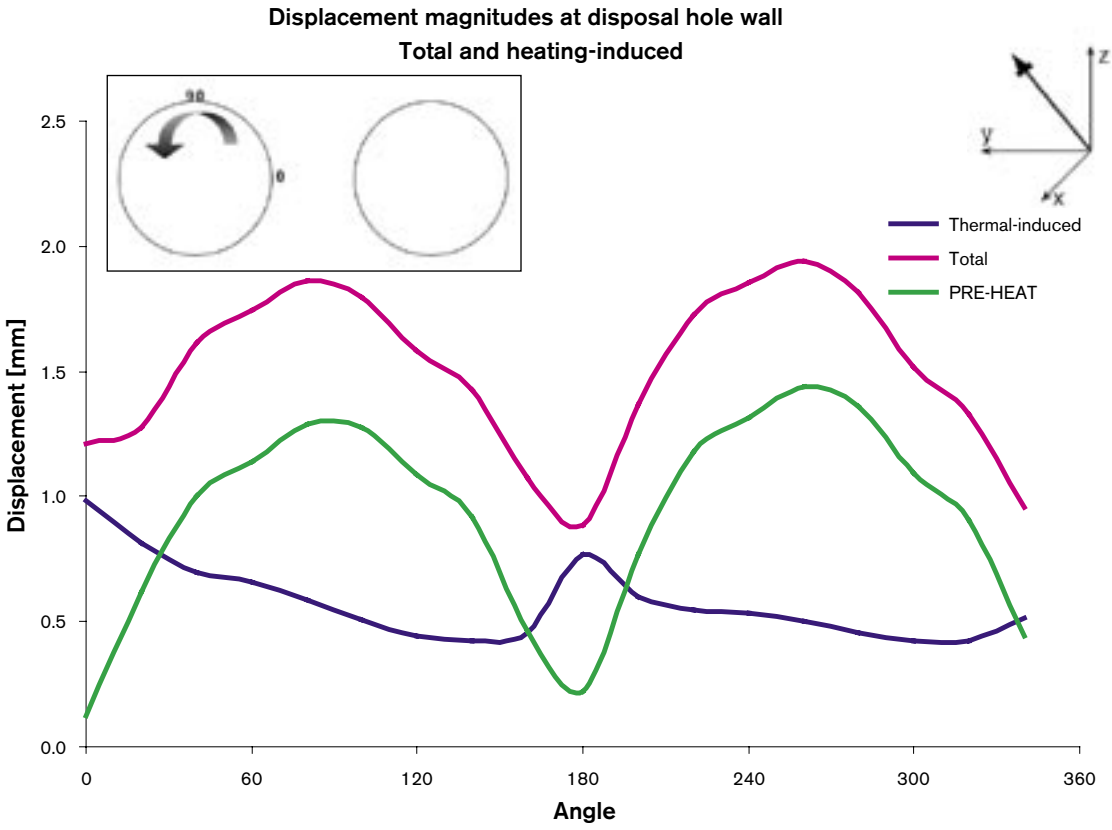

Figure 3-15. *Displacement magnitudes at the hole wall 0.5 m below the tunnel floor. Total displacement is the sum of pre-heat and thermal-induced displacements.*

3.5 Analyses

The uniaxial strength of the rock is 210 MPa, the crack damage stress 204 MPa, and the crack initiation stress 121 MPa. Figure 3-16 shows the crack initiation exceeding at the two level of interest. The uniaxial crack initiation stress is exceeded in both cases and the areas are quite large. However, the uniaxial crack damage stress is exceeded only at the very top of the pillar (Note here that this is based on uniaxial conditions/case which is not the actual situation).

The actual stress state at the pillar is true triaxial. To determine the effect of confining pressure few triaxial compression tests were conducted /Staub et al. 2004/. Based on test data four strength regions were identified; elastic, stable crack growth, permanent damage, and immediate failure regions. Stress-strength envelopes were composed assuming simplified linear relationship in σ_1–σ_3 space and assuming the set uniaxial strength values as said in Table 2-1. The envelopes indicate that e.g. when confining pressure (minor stress) increases from 0 to 10 MPa the strength increases about 28%. The composed stress-strength envelopes are shown in Figure 3-17.

The FLAC3D model was then analyzed with the obtained stress-strength relationship. Figure 3-18 shows the analysis outcome as marked regions based on stress state and strength within each element in FLAC3D model. Only stable crack growth regions (i.e. crack initiation stress exceeding) were identified and they reached two meters down the hole wall. These are the areas where damage may occur during the in-situ test. When the other hole is pressurized with 0.8 MPa confining pressure it yields from the stress-strength envelopes that the rock strength is 5 MPa (crack initiation 2.5% – peak strength 4.0%) higher than without confining pressure.

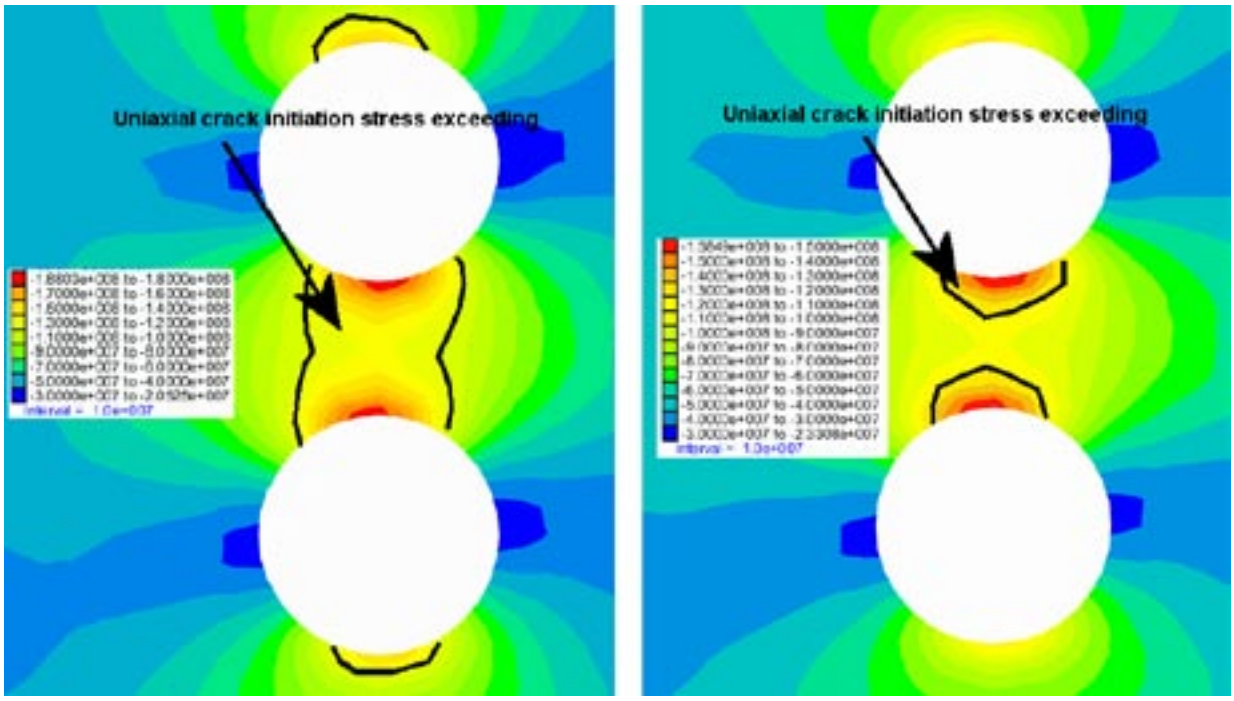

Figure 3-16. *Uniaxial crack initiation stress exceeding is enclosed with black line. Stress field after 120 days heating. Left horizontal cross-section 0.5 m and right 1.5 m below the tunnel floor.*

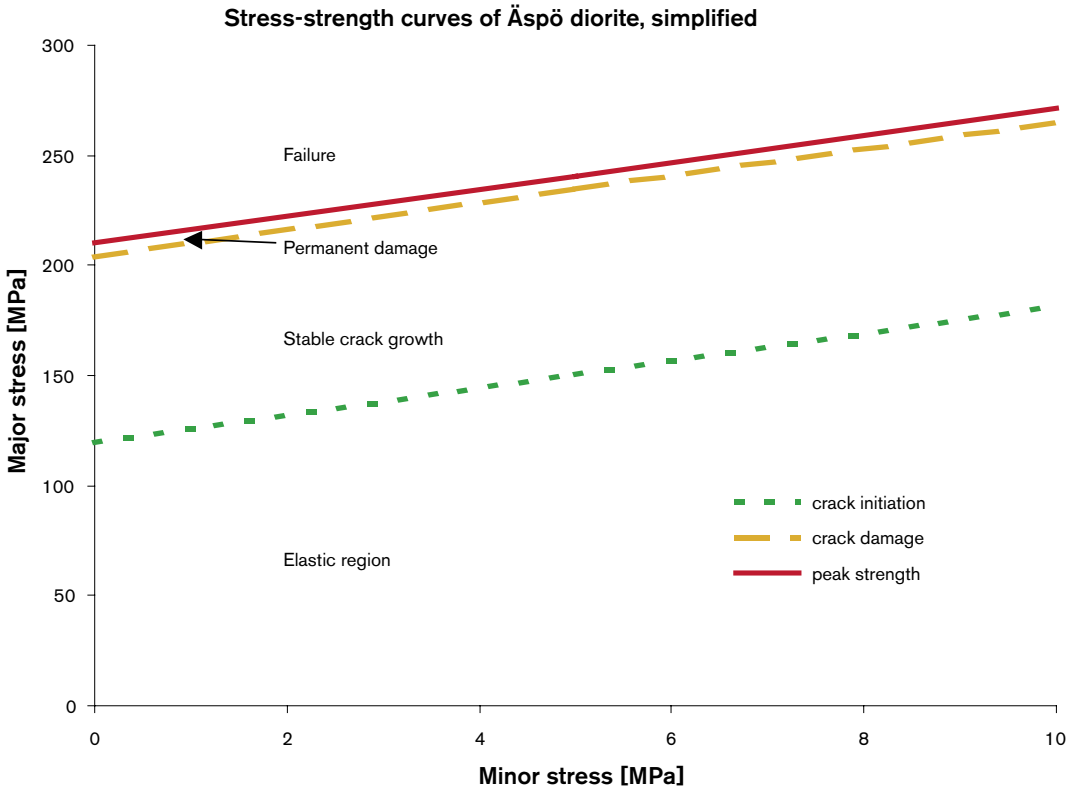

Figure 3-17. *Stress-strength envelopes used in model analysis assuming linear curve fitting based on laboratory triaxial test data and fixed uniaxial strength values.*

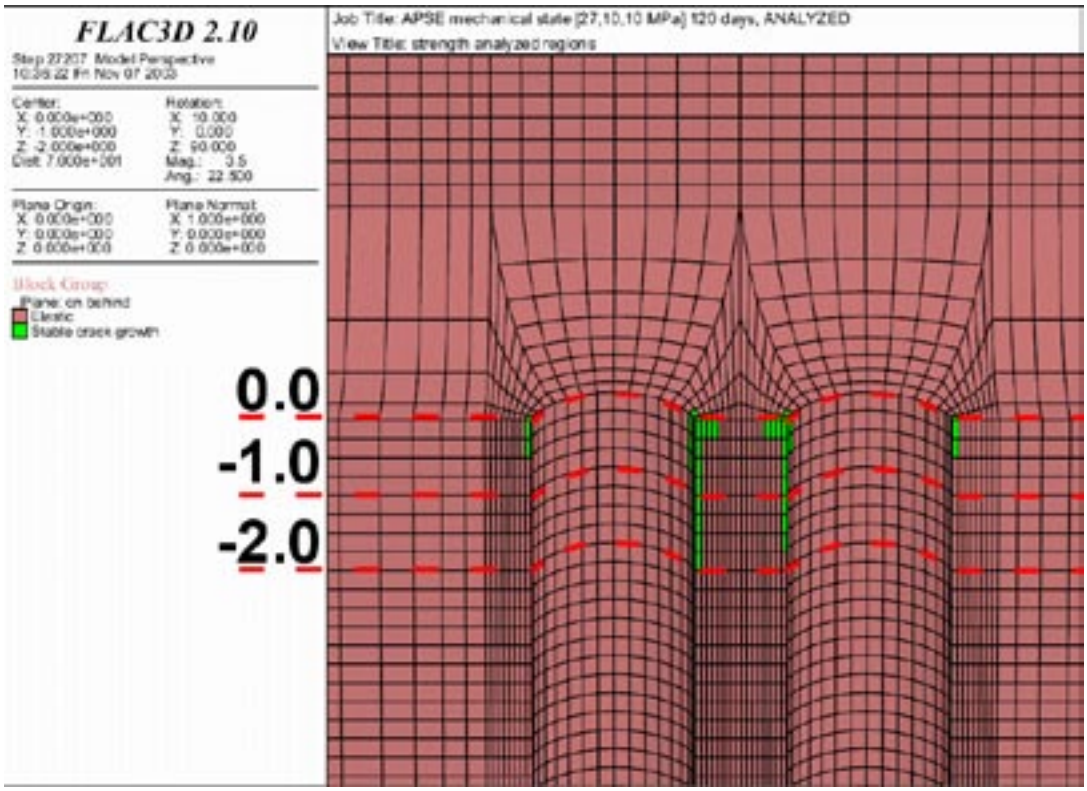

Figure 3-18. *Regions identified after heating in stress-strength analysis. Stable crack growth areas (crack initiation stress exceeding) reach down to about 2 meters.*

The crack initiation stress exceeding has some relationship with the acoustic emission activity, as it is the state where reversible microcracking occurs than could be detectible with AE-equipment.

It is to be noted that the amount of data used to compose the failure criterion is very limited. Only 14 specimens were tested using four different confining pressures (0, 1, 2, 7 MPa), so there were only about 2–4 specimens for each confinement. In addition, the tested rock specimens were (intact) diorite, which may overestimate the rock strength regarding the test site.

Sensitivity analyses were performed earlier in /Wanne and Johansson, 2003/. They showed that the modeled stresses are to some extent dependent on the used parameter values. As the thermal conductivity increased by 15% the stresses decreased by 4%. Moreover, when the modulus value was increased by 45% the stresses increased 13%. This holds only for thermal part of the modeling. When the thermal effect is neglected, the modulus change does not affect the stresses.

4 Coupled FLAC-PFC2D modeling

4.1 Background

Elastic FLAC3D model gives the stress field and elastic displacements around the tunnel opening and implies damage around holes from elastic stresses and known strength (see Section 3.5). However, in order to study in detail the damage that might occur another approach has to be taken. One possible and tested tool to model fracturing is based on discrete element method that uses circular or spherical shaped elements – called Particle Flow Code (PFC). First version of the code was introduced in 1995 by Itasca, the current version number is 3.0 /Itasca, 2003/. There are great number of studies that promote the use of PFC to model damages and fracturing in rock /Autio et al. 2002; Hazzard et al. 2000; Li and Holt, 2001; Potyondy and Cundall, 2004/.

4.2 Particle Flow Code

Particle Flow Code in 2 Dimensions (PFC2D) models mechanical behavior by representing a solid as a bonded assembly of circular particles. PFC2D models are categorized as direct, damage-type numerical models in which the deformation is not a function of prescribed relationships between stresses and strains, but of changing microstructure. /Itasca, 2003/.

The fundamental element in PFC2D is a circular particle. When the problem to be modeled concerns the interaction of circular particles, the code can be applied in a straightforward way. On the other hand, when modeling solid material such as rock, the application process is more complex as particle properties cannot be determined directly – they have to be interpreted in an iterative manner from the results of standard laboratory tests. The parameters required are called micro-properties. They dictate how the model will respond and the kind of macro-properties that it will output. In rocks, the micro-properties that produce the known macro-properties and observed behavior are not usually known. Although the behavior of the PFC2D model is found to resemble that of rock, generally the particles in a PFC2D assembly are not associated with the minerals or grains in rock. /Itasca, 2003/.

Calibration is the term used to describe the iterative process of determining and modifying the micro-properties for a PFC2D model. In the calibration process, the responses of the model are compared to the responses of the rock samples in the laboratory and the micro-properties of the model are modified in an iterative way to achieve good agreement. Comparisons can be at both laboratory and field scale. The laboratory-scale properties chosen for comparison were Young's modulus (E) and the unconfined compressive strength (UCS). The laboratory response used as a target for calibration is presented by /Staub et al. 2004/. For interested readers, /Kulatilake et al. 2001/ discuss general issues concerning the calibration of micro-mechanical properties for an intact model material using PFC.

4.3 Coupling of PFC and FLAC

PFC has been used as a stand-alone application to model damage processes in a small-scale. However, in APSE there is a need for large-scale model to take account the complex stress state and to include the whole pillar area in the model. If the entire model was made with PFC alone the computer resources and computing time needed would have been enormous. In order to overcome this restraint a coupled modeling approach was chosen.

The coupled model is made up of two-dimensional PFC region, which is enclosed by two-dimensional FLAC region. FLAC is a two-dimensional version of the FLAC3D software as described in Section 2.1. The coupling makes it possible to model in large-scale fracturing process of the pillar area and still limit the needed computational requirements.

The coupled model had an average Young's modulus of about 65 GPa and Poisson's ratio 0.23. The measured uniaxial peak strength of PFC2D was about 220 MPa and crack initiation stress about 104 MPa.

4.3.1 Coupling scheme

The coupling scheme embeds a PFC2D inclusion region within a FLAC grid. The applied forces received from PFC2D act on the grid points along the inclusion boundary. The masses of these grid points are increased to insure stable integration of the equations of motion. A PFC2D material is created to confirm to the shape of the inclusion region such that a single layer of particles overlaps the inclusion boundary. The translational velocities of these boundary particles are received from FLAC, and the reaction forces of these boundary particles are sent to FLAC. Figure 4-1 shows a schematic view of the coupling process.

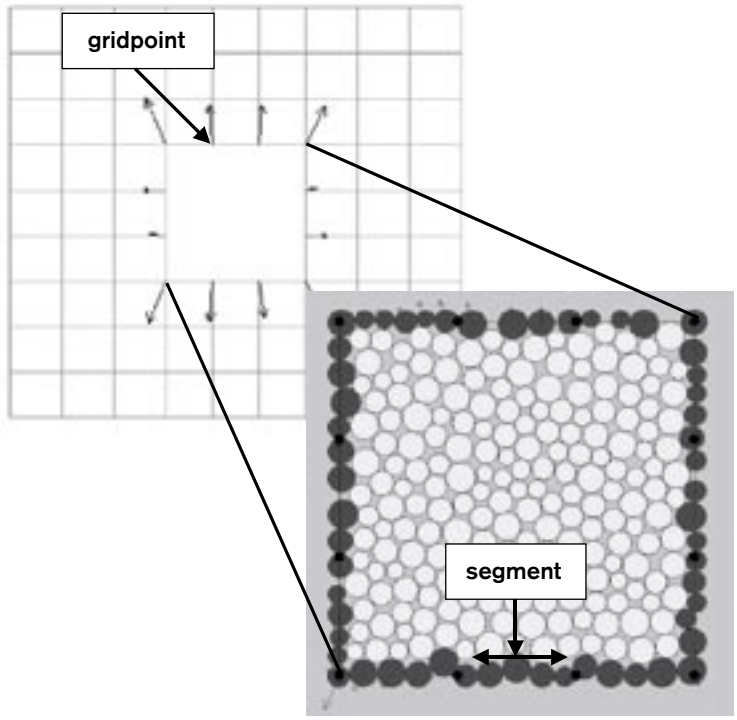

Figure 4-1. *Schematic view of the PFC-FLAC coupling process.*

Communication between the codes occurs via a socket connection (as used for TCP/IP transmission over the Internet), which allows data contained in arrays to be transmitted in binary with no loss of precision between the two codes running as separate processes. The codes may be on the same machine, or on two different machines on the same network.

Cycling in both codes is synchronized such that one system step consists of each code taking a step, with PFC2D receiving velocities before its motion calculation and sending forces after its force-displacement calculation and FLAC sending velocities and receiving forces after its motion calculation. The timesteps in both codes are identical. This is achieved by running FLAC in static mode and PFC2D with density scaling so that the timestep is unity for both processes.

4.4 PFC-FLAC model for APSE

Coupled PFC2D-FLAC (PAC) is a two-dimensional modeling environment. Thus pillar stability modeling was performed in one plane of interest; 0.5 m below the tunnel floor. Plane strain (ε_z=0) assumption was used in the modeling. Because the stresses around the experimental area are disturbed and therefore difficult to implement, the stresses were queried from the existing three-dimensional FLAC3D model via aforementioned socket connection, as well as temperature fields, at different points of time (30, 60, 90, 120 days of heating). The coupling between FLAC3D and PAC is one-way; FLAC3D sends queried stress/temperature data, but the actual modeling calculations are performed only in FLAC and PFC. Schematic view of the entire coupled system is shown in Figure 4-2.

FLAC has about 6,000 zones and spreads out 18 m by 12 m. The embedded PFC model consists of about 65,000 particles with the average particle diameter of 22 mm. The width of the PFC specimen is 6.4 m and height 3.6 m.

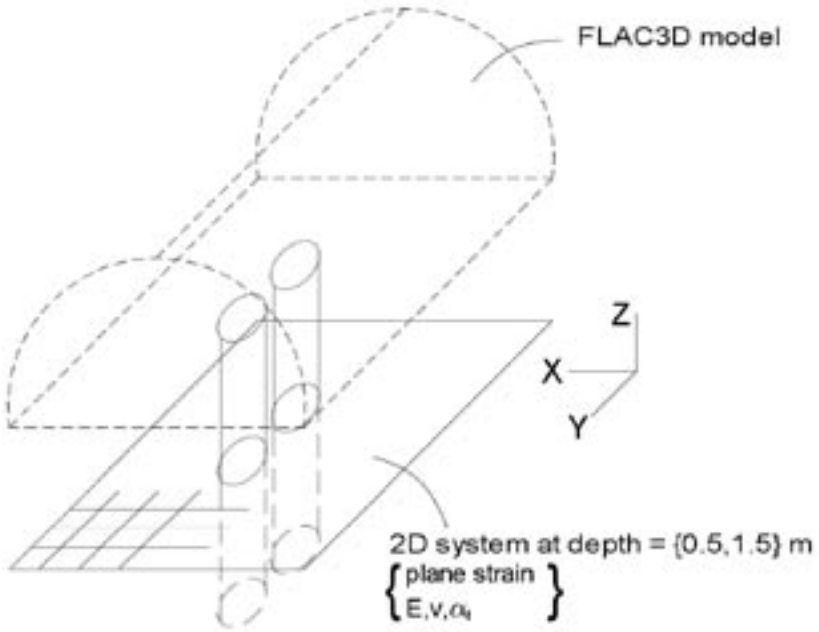

Figure 4-2. *Coupled system in APSE. PFC and FLAC are computationally fully coupled, FLAC3D connection is unidirectional.*

4.5 Coupled model results

Figure 4-3 shows forces in the pillar area after boring of the hole. Most of the pillar area is in uniaxial compressive condition. There are random scattered microcracking around the pillar but they have not coalesced into an actual fracture. As the heating starts and, thus, stresses increase more microcracking starts to appear. Fractures of different stages of heating are shown in Figures 4-4 through 4-7. The cracking concentrates at the hole wall as the induced stresses start to exceed the material strength. The microcracks begin to localize and finally form a predominant fracture at the hole wall. At the highest stress conditions small fragments of the pillar wall are loosened and falling to the experimental hole.

If the stresses become higher than expected or the strength of the pillar is lower, damage that may occur is more extensive. With the exaggerated circumstances notches form at the pillar (Figure 4-8, top). Finally, if the situation is favorable, fractures penetrate into the pillar as seen in Figure 4-8, bottom.

The formed microcracks are localized and forming asymmetrically distributed fractures around the holes. The exact extent of failures cannot be determined as there are no detailed data available from the pillar area in order to adjust the model. These results indicate that some fractures shall be generated in rock and failures may then occur.

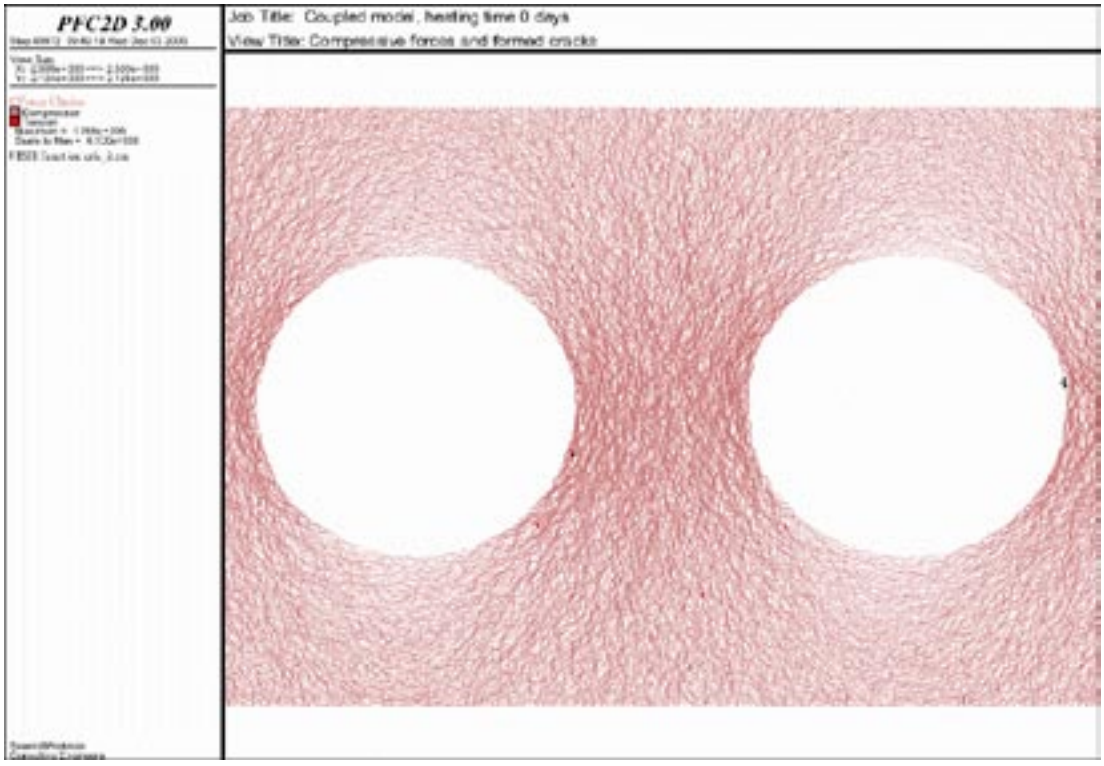

Figure 4-3. *Forces between the particles. Vector width is proportional to the magnitude of the effective force. Pillar area is loaded mainly in compression. Upper part of the hole wall is nearly unloaded or in tension (black=tension, red=shear).*

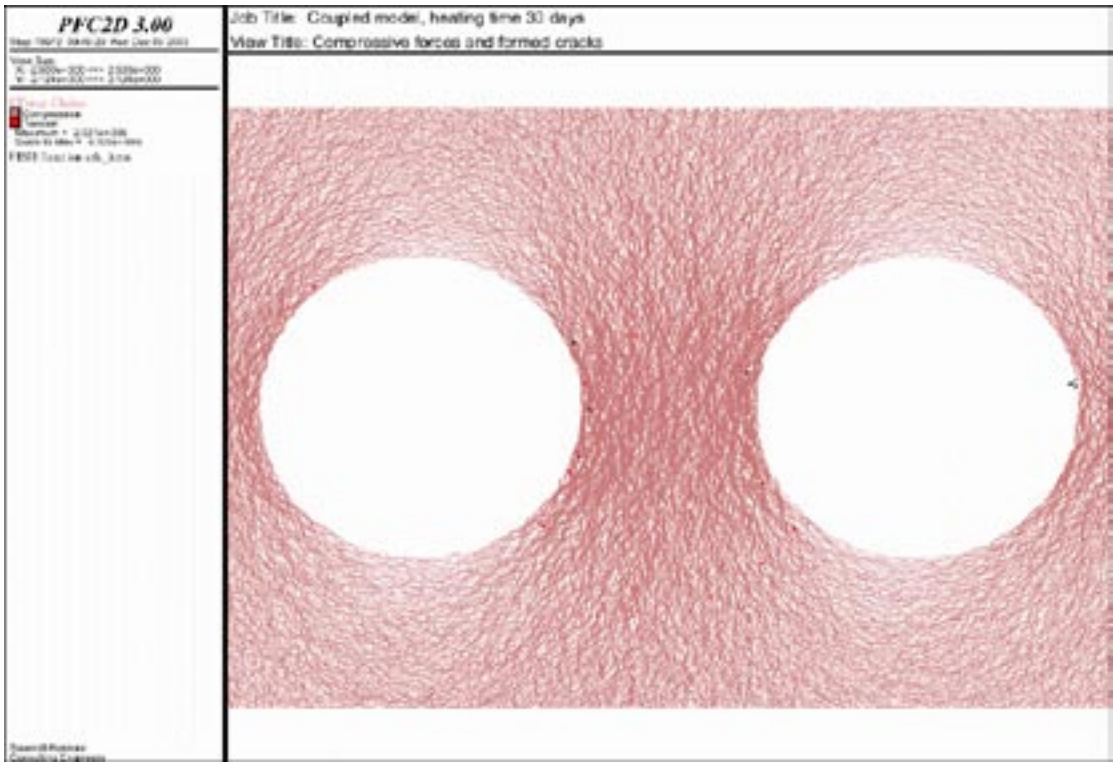

Figure 4-4. *Forces and cracking between the particles after 30 days of heating. Vector width is proportional to the magnitude of the effective force. Cracking is concentrating in the pillar at the hole surface. Number of cracks 25, (black=tension, red=shear).*

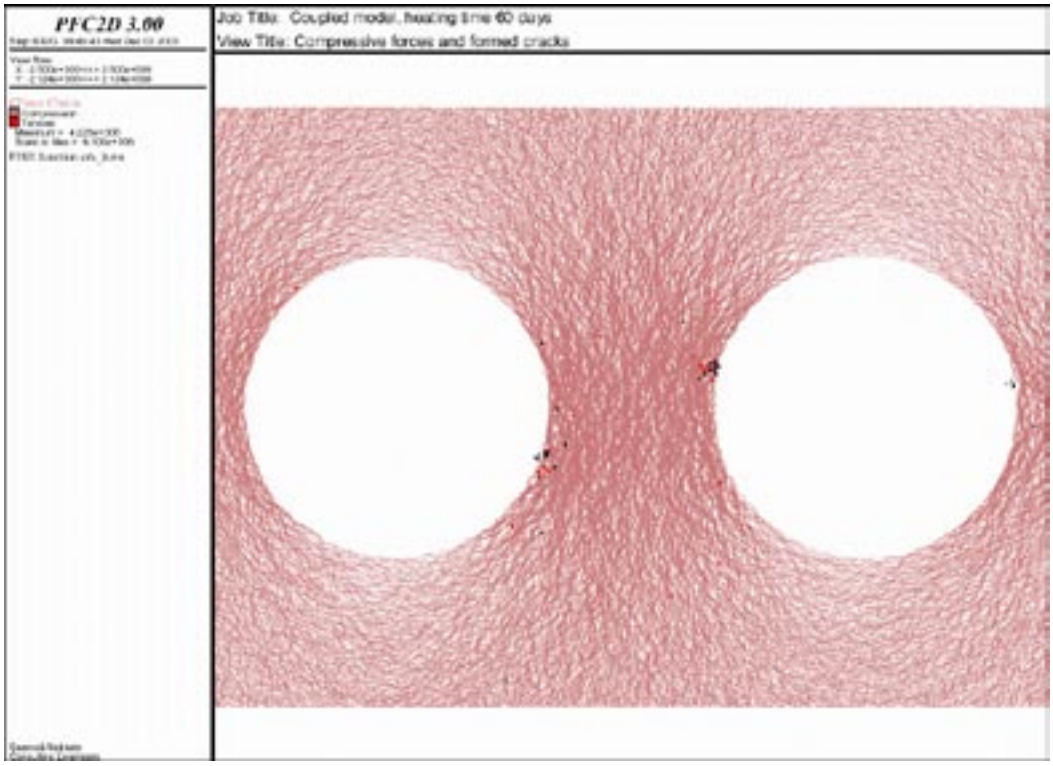

Figure 4-5. *Forces and cracking between the particles after 60 days of heating. Vector width is proportional to the magnitude of the effective force. Cracking is concentrating in the pillar at the hole surface. Number of cracks 68 (black=tension, red=shear).*

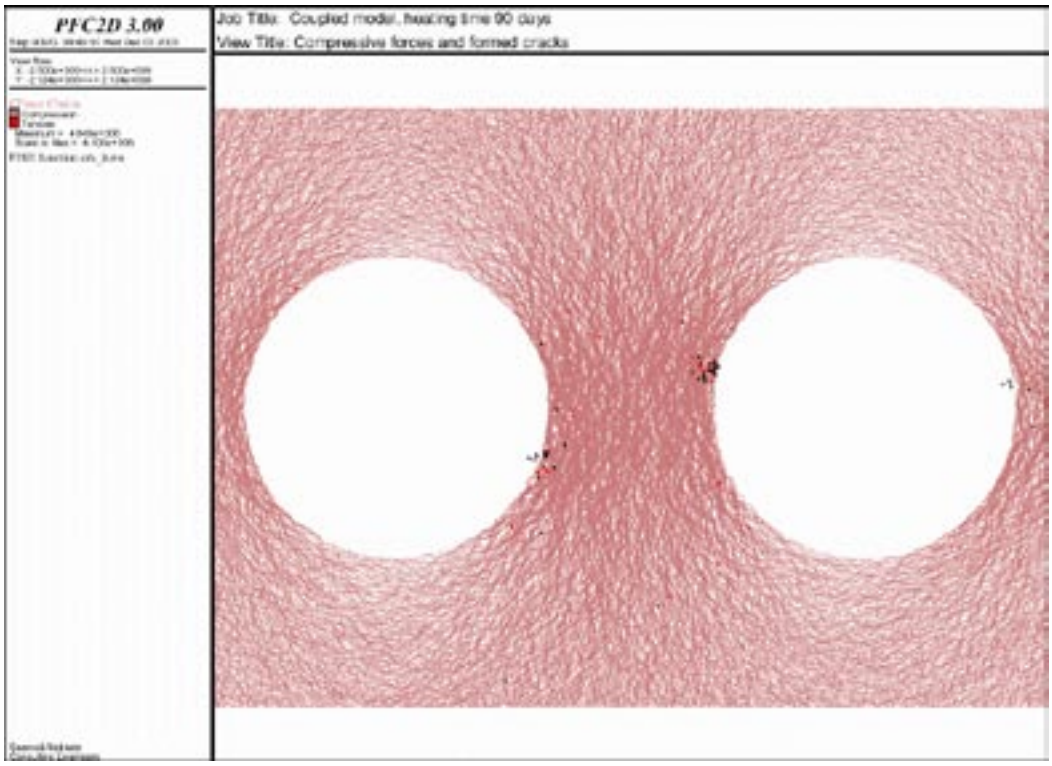

Figure 4-6. *Forces and cracking between the particles after 90 days of heating. Vector width is proportional to the magnitude of the effective force. Cracking is concentrating in the pillar at the hole surface. Number of cracks 83 (black=tension, red=shear).*

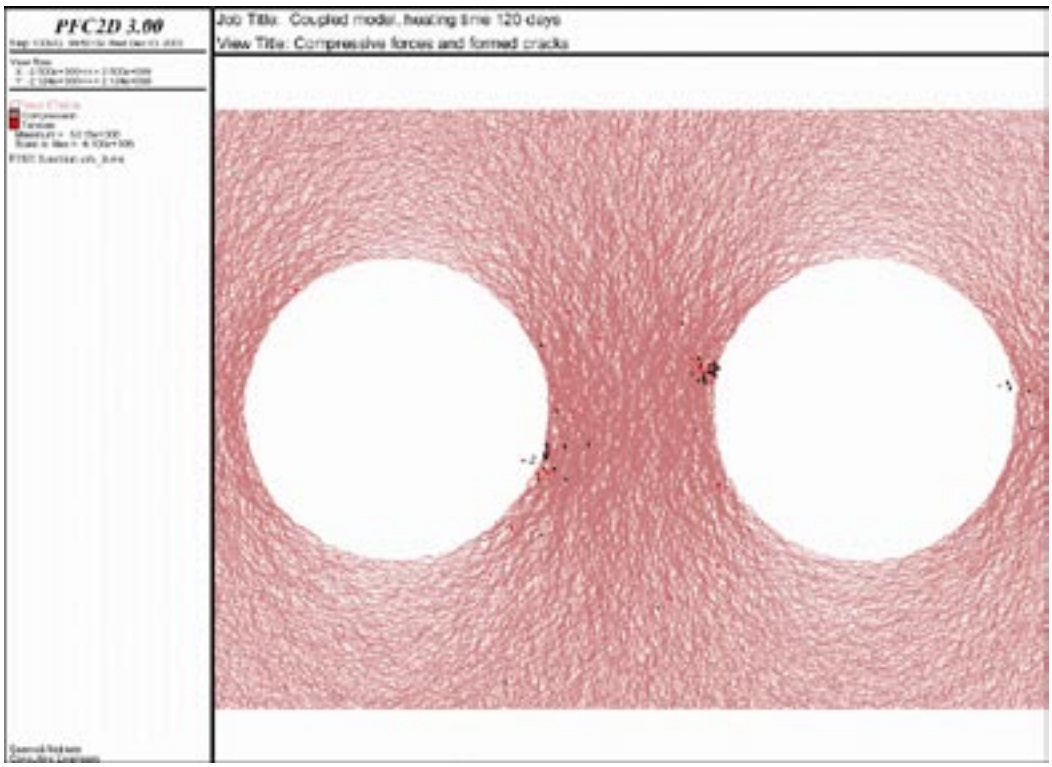

Figure 4-7. *Forces and cracking between the particles after 120 days of heating. Vector width is proportional to the magnitude of the effective force. Cracking is concentrating in the pillar at the hole surface. Number of cracks 91 (black=tension, red=shear).*

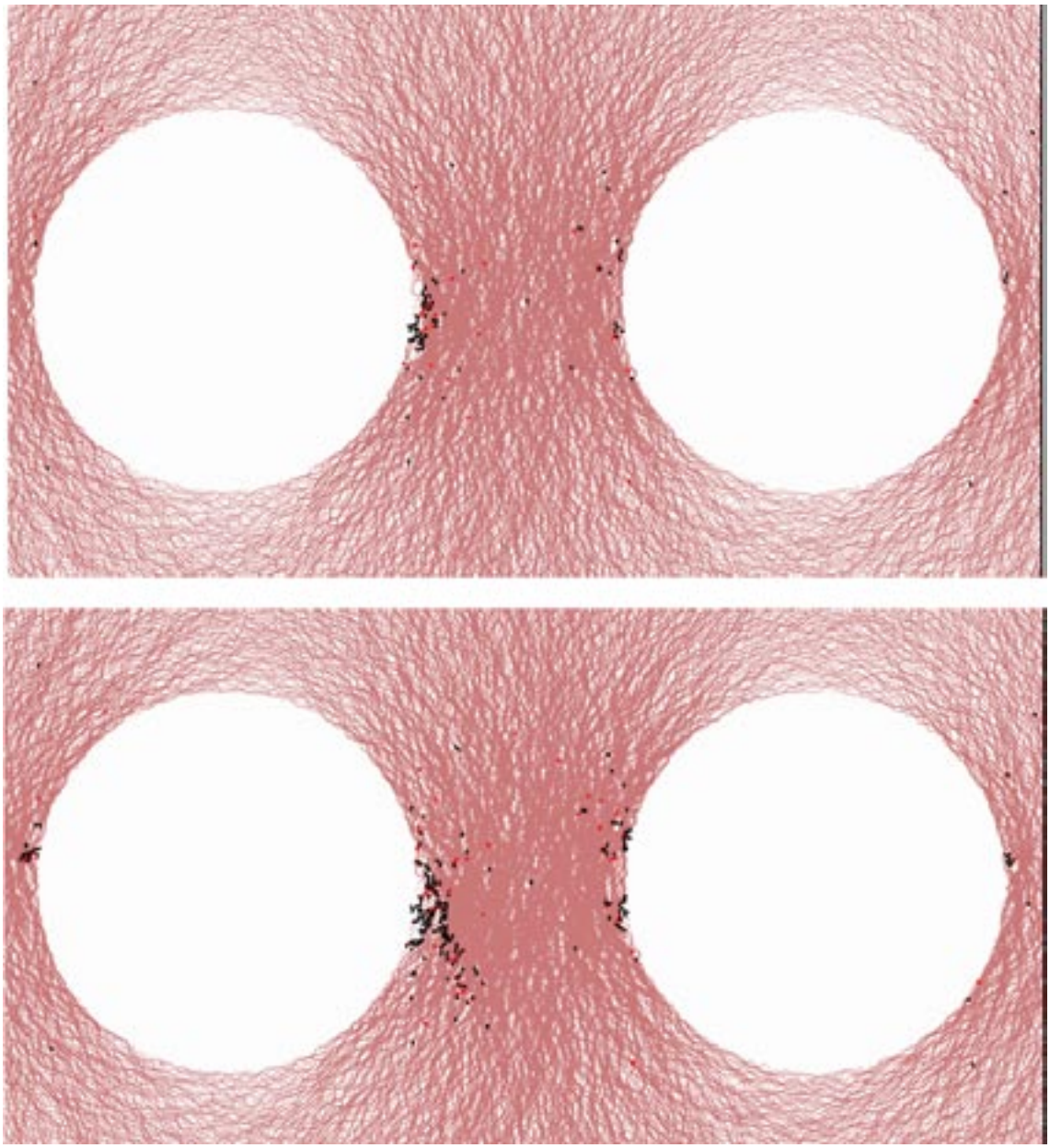

Figure 4-8. *Damages at pillar if the circumstances are unfavorable (stresses higher, strength lower) (black=tension, red=shear). Number of microcracks 117 (upper) and 304 (lower).*

4.6 Scale effect in PFC modeling

Significant parameter when using coupling to model large-scale excavation response is strength of the material. As the model is calibrated using data from laboratory scale tests some modification is needed to take account the scale effect. When PFC is used to model laboratory scale events no modification is needed as experiences in the past have shown. There is analog to a simple uniaxial test on rock. When the specimen size is increased, the strength of the corresponding rock specimen is reduced. With larger specimens more naturally existing flaws, microcracks and pores are included, and hence the specimen is weaker. This issue in PFC modeling has not been widely studied yet. /Potyondy and Cundall, 2004/ provide some discussion about the issue in URL related modeling:

No significant damage forms as a result of excavation in any of the PFC simulations of the Mine-by Experiment; however, application of a strength-reduction factor of 0.6 to the material produces a stable breakout notch. The notch-formation process is sensitive to the strength-reduction factor. It is not clear what procedure should be used to calibrate the strength-reduction factor, other than comparing the final extent of any notches that form in boundary-value models of excavations. The use of a uniform strength-reduction procedure to predict excavation damage may be limited to qualitative assessments of the nature of the possible damage, and use of a properly calibrated stress-corrosion model may be required to make quantitative assessments. The fact that similar notches form for both strength-reduction procedures supports such use of a uniform strength reduction approach.

/Potyondy and Cundall, 2004/ continue on adjusting the microstrengths:

We still do not know exactly what is the mapping between specimen-size behavior and field-scale behavior. This manifests itself in PFC models. To get a reasonable failure micro-strengths have to be scaled down. The scaling down accounts for the fact that the true pillar may have micro-defects, etc. that are not present in initial very well-connected and perfectly constructed PFC2D material. This is an unresolved issue for PFC modeling of boundary-value problems.

In the coupled modeling the strengths of the particle-particle bonds of the PFC material was reduced. The particle bond strengths were multiplied by a factor of 0.6 (a factor of 1.0 refers to original value and 0 to no-strength) to reduce strength of the material.

5 Comparisons of models

Results of the latest FLAC3D model were compared with the results of the previous modeling. In addition, FLAC3D results were compared with the PFC-FLAC results.

The current FLAC3D modeling was performed with updated input data collected from the actual in-situ test site (tunnel logging, convergence measurements and laboratory tests). Data used in earlier modeling was gathered from different sources and locations around the Äspö HRL (see /Wanne and Johansson, 2003/ for details). Figure 5.1 compares the crack initiation stress exceeding in new and old FLAC3D model at the level of 1.5 meters below the tunnel floor. Main differences in the input data were in the in-situ stress field and the thermal properties. Despite the differences in the initial modeling, data the overall results are quite similar. The highest compressive stress region is located at the whole surface with the magnitude of around 150 MPa. The earlier model showed that there are small tensile areas around the whole perimeter. The modeling made with the updated data show that no tensile areas exist around the hole after the heating. Rock around the holes is in compression state.

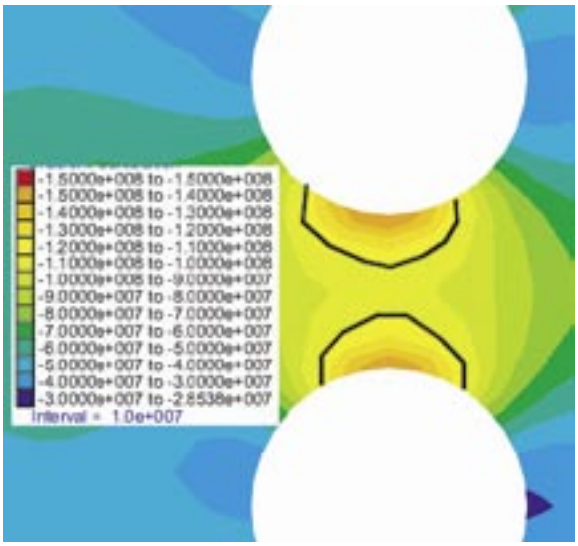

In-situ stress field [MPa]
25,15,10, Max induced stress 150 Map
Linear exp. coeff., α_t [1/°C]
7.9×10^{-6}
Young's modulus, E [GPa]
68.0

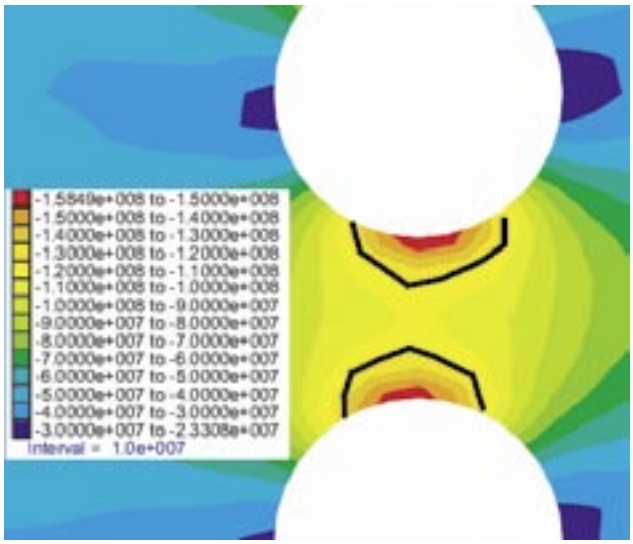

In-situ stress field [MPa]
27,10,10, Max induced stress 158 MPa
Linear exp. coeff., α_t [1/°C]
7.0×10^{-6}
Young's modulus, E [GPa]
55.0

Figure 5-1. *Uniaxial crack initiation stress exceeding. Comparison of the FLAC3D results between earlier and current modeling. Main differences in input data are also presented. New analysis on right, old on left. After 120 days of heating, 1.5 m level.*

Comparison was also made between FLAC3D and coupled PFC2D-FLAC results in a horizontal plane 0.5 meters below the tunnel floor (Figure 5-2). The cracking in PFC, which formed due the thermal-induced load increase, was located at the hole surface region. Same regions were identified by stress-strength analyses by FLAC3D, which took into account the prevailing triaxial stress state at the pillar area. The crack concentration areas were about 10 cm deep in FLAC3D. Visible spalling could be noticed in PFC model (by detached particle clusters).

Elastic FLAC3D model indicates that there are elements where damage might occur and PFC2D model shows actual fracturing/damages and crack propagation.

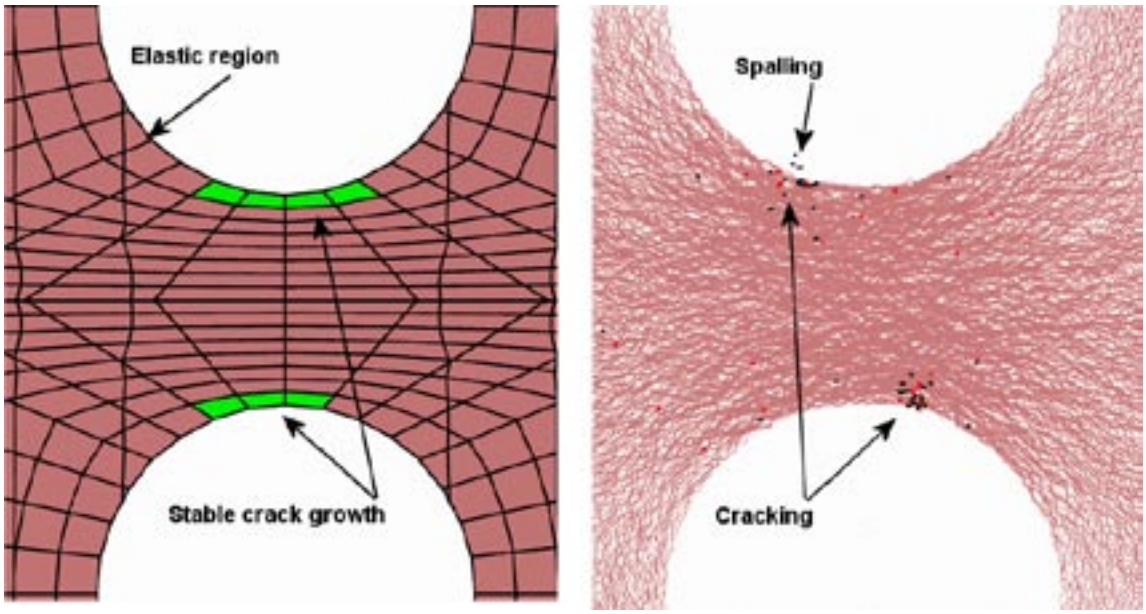

Figure 5-2. *FLAC3D analyzed stress-strength regions and PFC2D cracking location and extent.*

6 Predictions

SKB assigned the task to make specific spalling predictions by giving the four questions listed below:

1. What is the failure criterion, i.e. where does one obtain spalling?
2. What tangential stress is required to initiate spalling?
3. How deep will the spalling propagate as a function of stress, i.e. how depth of failure?
4. What is the effect of confining stress on 1, 2 and 3 above?

This section is the FLAC3D interpretation to these questions.

6.1 What is the failure criterion for spalling, i.e. where does one obtain spalling?

It should be noted here that in the report by S&R we don't exactly discuss failure criterion for spalling but the stress levels when the damage (=crack initiation stress) starts to take place in the rock. Failure envelopes were composed assuming simplified linear relationship in σ1–σ3 space using the uni- and triaxial lab tests conducted by HUT. In addition, the following assumptions were used a) the crack initiation stress at σ_3=0 was fixed and given by SKB to be 121 MPa and b) the gradient for σ_{ci} was assumed to be similar than for peak strength (although the gradient is much lower based on lab tests, see Figure. 6-1). The composed stress-strength envelope is shown in Figure 6-1. (Figure 3-17). In the FLAC3D model only areas where σ_{ci} exceeded were identified (Figure 3-18).

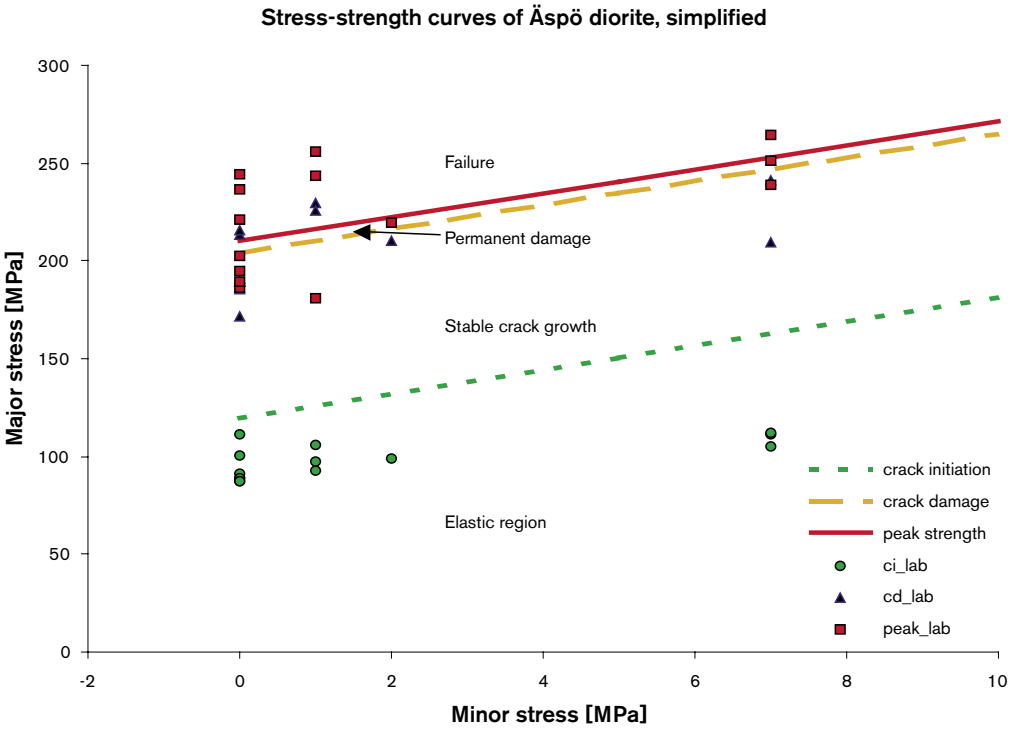

Figure 6-1. *Failure envelopes used in the analyses in the final report.*

6.2 What tangential stress is required to initiate spalling?

Based on above the tangential stress at hole wall to initiate damage is 121 MPa at σ_3=0 (see note in item 3 on stresses at hole wall).

6.3 How deep will spalling propagate as a function of stress, i.e. depth of failure?

The damage areas extent about 1.7 meters down to the hole. The depth of the damaged area is about 0.25 m and the width about 0.8 m on the top and 0.08 m and 0.4 m at the tip, respectively. It should be noted that the estimation of the damage area is controlled over the model element size in the pillar, which is about 5 × 15 × 25 cm (Figure 3-20 in the report). It should be also noted that the calculated stresses are average values in the center of a zone thus not giving the correct value at the hole wall. This slightly underestimates the damage area.

6.4 The effect of confining stress on 1, 2 and 3?

All the above are based on the triaxial situation. The confining stress has a clear effect on the damage areas as shown in Figure 3-17 in the report. The failure envelope (Figure 6-1) indicates that e.g. when confining pressure (minor stress) increases from 0 to 0.8 MPa the crack initiation stress increases by about 4% (121 to 125 MPa).

6.5 Discrete damage modeling

As there are few issues (as stated in the report) related to the use of the coupled PFC2D-FLAC system that clearly affected the predicted damages, no prediction of spalling was made based on PFC-FLAC analyses.

7 Summary

The maximum principal stress at the top of the pillar before any heating is about 150 MPa due the geometry and orientation of the tunnel and hole excavation.

The initial temperature rises from 15°C to about 65°C in the pillar area during the heating period of 120 days. The rising temperature induces stresses in the pillar area and after 120 days heating the stresses have increased about 33% from 150 MPa to 200 MPa. Figure 7-1 shows the increase of the stress at the two levels during the 120 days heating. Figure 7-2 presents the compressive stresses at a straight line between the two holes. Largest stress values are found at the hole surfaces (both ends of the line).

The presented rock strength properties are based on 14 laboratory tested specimens taken from the actual test site. The uniaxial crack initiation stress (σ_{ci} ~ 121 MPa) is exceeded before the heating at the upper part of the pillar. Crack damage stress (σ_{cd} ~ 204 MPa) is exceeded at the top of the pillar after the heating. Peak strength (σ_p ~ 210 MPa) is not exceeded in any stage.

It should be noted that the strength values presented here correspond to an uniaxial stress state and in true polyaxial situation the strength values are higher e.g. the peak strength of Äspö diorite is about 250 MPa with confinement of 7 MPa. The used values may also overestimate the strength behavior of the rock mass (Section 3.5).

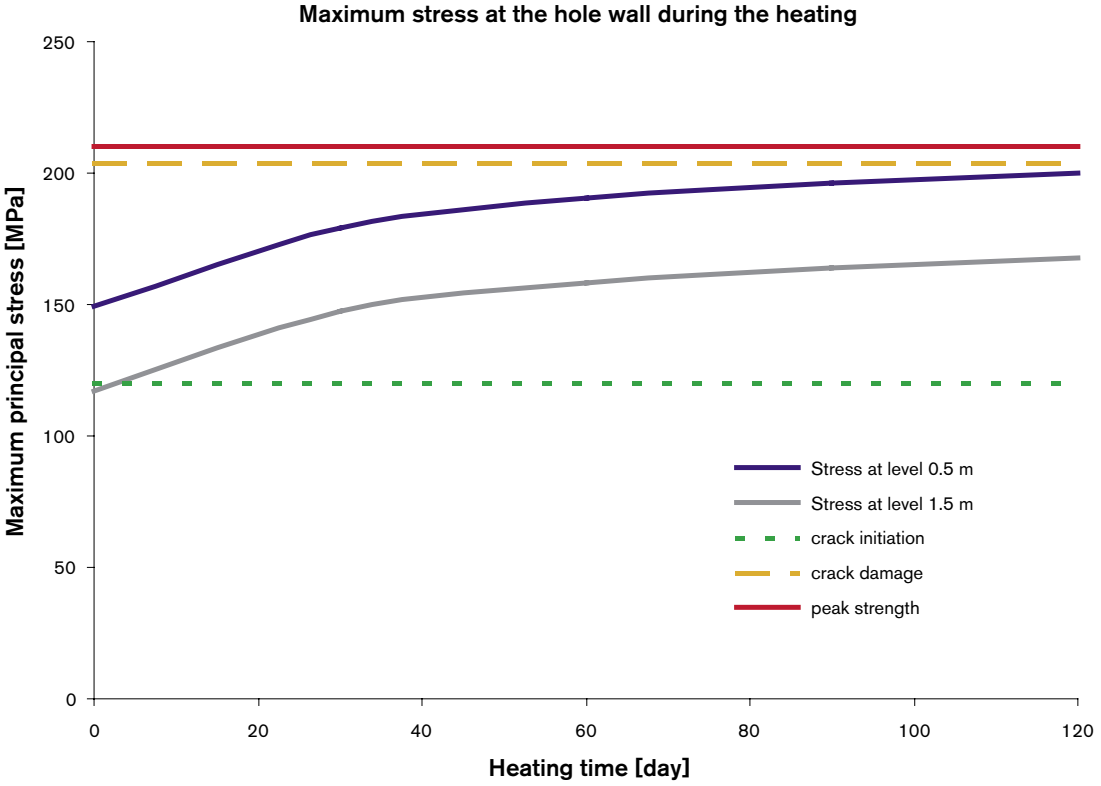

Figure 7-1. *Stress at the hole wall during the 120 days heating at the levels of 0.5 m and 1.5 m below the tunnel floor.*

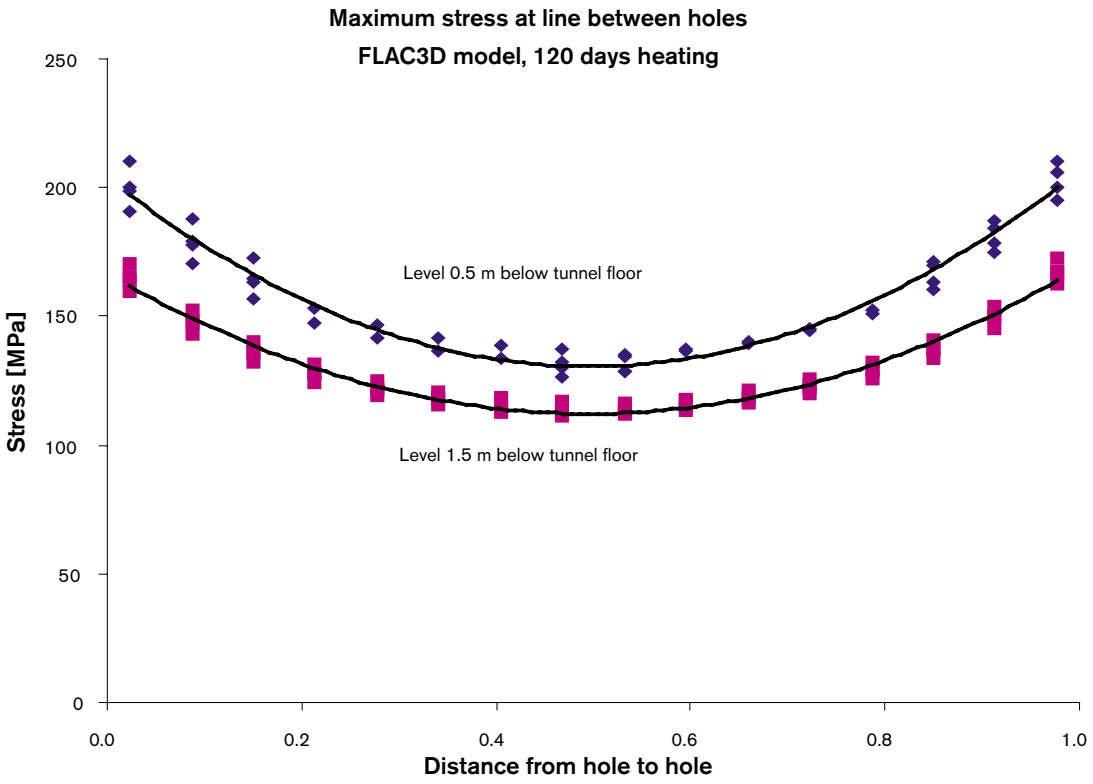

Figure 7-2. *Maximum compressive stresses along a straight line between the holes at two levels.*

The minor tensile stress areas are located at hole sidewalls. The areas exist before the heating starts and are lessening when the heat is on. Tensile stresses in addition to high compressive stresses might induce some AE activity from the very beginning of the test and are thus potential areas where AE activities will be detected.

Earlier models made with solely PFC in laboratory-scale and comparison to the actual laboratory tests have shown that PFC could simulate fracturing and damaging of rock samples. The novel coupling between PFC and FLAC were successful and the obtained results outline the damage process during the in-situ test. However, the material model used with PFC needs further development and was outside of the scope of this study.

Particle-mechanical model has demonstrated its ability to model fracturing and damage forming of rock realistically. The main restriction is the huge computational resources needed when modeling a true 3D environment. Development a new fully three-dimensional numerical code based on PFC represents a significant advance over current numerical modeling approaches and will have a wide range of application for example in underground engineering. The code makes it possible to study in detail cracking and failure mechanisms in highly stressed regions of interest. As the model is fully three-dimensional it enables full quantitative validation against field and laboratory observations. /Young, 2003/.

8 References

Andersson J C, 2003. Äspö Pillar Stability Experiment, Summary of preparatory work and predictive modelling. SKB R-03-02, Svensk Kärnbränslehantering AB.

Autio J, Potyondy D, Wanne T, 2002. Particle mechanical simulation of the effect of schistosity on strength and deformation of hard rock. In Proceedings of the NARMS-TAC2002 Conference, Toronto, July 2002. University of Toronto Press. Canada.

Barton N, 2003. Äspö Hard Rock Laboratory. Äspö Pillar Stability Experiment. Q-logging of the APSE Tunnel at Äspö. For rock quality assessment and for development of preliminary model parameters. SKB IPR-04-07, Svensk Kärnbränslehantering AB.

Fredriksson A, Staub I, Janson T, 2003. Äspö Hard Rock Laboratory. Äspö Pillar Stability Experiment. Design of heaters and preliminary results from coupled 2D thermo-mechanical modelling. SKB IPR-03-03, Svensk Kärnbränslehantering AB.

Hazzard J, Young P, Maxwell S, 2000. Micromechanical modeling of cracking and failure in brittle rocks. Journal of geophysical research. Vol 105. No. B7, p. 16,683–16,697.

Itasca Consulting Group Inc, 2002. FLAC3D (Fast Lagrangian Analysis of Continua in 3 Dimensions). Version 2.1. Minneapolis. USA.

Itasca Consulting Group Inc, 2003. PFC2D. Particle Flow Code in 2 Dimensions. Version 3.0. Minneapolis. USA.

Kulatilake P, Malama B, Wang J, 2001. Physical and particle flow modeling of jointed rock block behavior under uniaxial loading. Int. J. of Rock Mech. and Min. Sci. Vol. 38. p. 641–657.

Li L, Holt R, 2001. Simulation of granular material using particle model with non-circularly shaped super-particles. Rock mechanics – a challenge for society. In Proceedings of the ISRM regional symposium Eurock 2001. A.A.Balkema. Netherlands.

Potyondy D, Cundall P, 2004. A bonded-particle model for rock. Int. J. Rock Mech. and Min. Sci. Special issue on Canada's Underground Research Laboratory (URL) contributions to rock mechanics. Vol. 41. p. 1329–1364.

Rinne M, Shen B, Lee H-S, 2003. Äspö Hard Rock Laboratory. Äspö Pillar Stability Experiment. Modelling of fracture stability by FRACOD. SKB IPR-03-05, Svensk Kärnbränslehantering AB.

Staub I, Andersson J C, Magnor B, 2004. Äspö Pillar Stability Experiment, Geology and properties of the rock mass in TASQ. SKB R-04-01, Svensk Kärnbränslehantering AB.

Wanne T, Johansson E, 2003. Äspö Hard Rock Laboratory. Äspö Pillar Stability Experiment. Coupled 3D thermo-mechanical modeling. Preliminary results. SKB IPR-03-04, Svensk Kärnbränslehantering AB.

Young R, 2003. An innovative 3-D numerical modelling procedure for simulating repository-scale excavation in rock – SAFETI. Impact of the EDZ on the performance of radioactive waste geological repositories. In Proceedings of a European Commission CLUSTER Conference, Luxembourg, November 2003. Pre-Print. To be published in the EUR series.

APSE publications

Andersson, J. Christer
Äspö Pillar Stability Experiment, Summary of preparatory work and predictive modelling. SKB R-03-02, Svensk Kärnbränslehantering AB.

Andersson, J. Christer and Martin, C.D. and Christiansson, R.
SKB's Äspö Pillar Stability Experiment, Sweden.
In the proceedings of Gulf Rocks 2004, the 6th North American Rock Mechanics Symposium (NARMS), Houston, Texas, June 5–9, 2004.

Andersson, J. Christer and Rinne, M. and Staub, I. and Wanne, T.
Stephansson, O. and Hudson, J.A. and Jing, L. (ed.)
The on-going pillar stability experiment at the Äspö Hard Rock Laboratory, Sweden.
In the proceedings of GeoProc 2003, International conference on coupled T-H-M-C processes in Geo-systems: Fundamentals, Modelling, Experiments & Applications. KTH, October 13–15, 2003, Stockholm, Sweden, p. 385–390

Andersson, J. Christer and Martin, C.D.
Katsuhiko Sugawara and Yuozo Obara and Akira Sato (ed.)
Stress variability and the design of the Äspö Pillar Stability Experiment. In the proceedings of the third international symposium on rock stress. RS Kumamoto '03, 4–6 November 2003, Kumamoto Japan, p. 321–326

Fredriksson, Anders and Staub, I. and Outters, N.
Äspö Pillar Stability Experiment, Final 2D coupled thermo-mechanical modelling. SKB R-04-02, Svensk Kärnbränslehantering AB.

Rinne, Mikael and Lee, H-S. and Shen, B.
Äspö Pillar Stability Experiment, Modelling of fracture development of APSE by FRACOD. SKB R-04-04, Svensk Kärnbränslehantering AB.

Staub, Isabelle and J.C. Andersson and B. Magnor
Äspö Pillar Stability Experiment, Geology and mechanical properties of the rock in TASQ. SKB R-04-01, Svensk Kärnbränslehantering AB.

Wanne, Toivo and Johansson, E. and Potyondy, D.
Äspö Pillar Stability Experiment, Final Coupled 3D thermo – mechanical modeling. Preliminary Particle – mechanical modeling. SKB R-04-03, Svensk Kärnbränslehantering AB.